Durham University

Durham E-Theses

Cu insertion into Cu-dependent nitrite reductase AniA from Neisseria gonorrhoeae.

RICHARDS, JOHN,HUGH

How to cite:

RICHARDS, JOHN,HUGH (2024) *Cu insertion into Cu-dependent nitrite reductase AniA from Neisseria gonorrhoeae.*, Durham theses, Durham University. Available at Durham E-Theses Online: http://etheses.dur.ac.uk/15725/

Use policy

The full-text may be used and/or reproduced, and given to third parties in any format or medium, without prior permission or charge, for personal research or study, educational, or not-for-profit purposes provided that:

- a full bibliographic reference is made to the original source
- a link is made to the metadata record in Durham E-Theses
- the full-text is not changed in any way

The full-text must not be sold in any format or medium without the formal permission of the copyright holders.

Please consult the full Durham E-Theses policy for further details.

Academic Support Office, The Palatine Centre, Durham University, Stockton Road, Durham, DH1 3LE
e-mail: e-theses.admin@durham.ac.uk Tel: +44 0191 334 6107
http://etheses.dur.ac.uk

Cu insertion into Cu-dependent nitrite reductase AniA from *Neisseria gonorrhoeae*.

John Richards

Master of Research Thesis
Department of Biosciences
Durham university

2024

Abstract

AniA is a copper dependent nitrite reductase expressed in pathogenic *Neisseria gonorrhoea.* It catalyses the first step of the denitrification pathway and is known to be important in gonococcal pathogenesis. The active protein is a homotrimer containing three T1Cu and three T2Cu sites. *In vivo* copper is inserted into these sites by metallochaperone AccA however little is known about how this process occurs. Though previous work indicates that the *apo*-form of AniA is a monomer, non-specific cleavage of AniA during protein purification hindered further research into the process.

This project therefore attempting to improve the protein purification process by changing the protease used during purification or eliminating its use altogether. These efforts where however unsuccessful as AniA for two reasons: AniA cannot be purified without a purification tag and AniA is highly susceptible to non-specific cleavage in its C-terminal domain. This suggests that this region is highly flexible in *apo*-AniA.

This project also investigated the insertion of aqueous copper into *apo*-AniA using fluorometry and UV-vis Spectroscopy. This showed that copper loading into the T1Cu site quenches the tryptophan fluorescence. It confirmed that copper inserts into T1Cu site before the T2Cu site and showed that the T1Cu site competes with NTA for copper providing a potential method for measuring the T1Cu sites affinity. Kinetic UV-vis spectroscopy studies suggested that copper loading occurs in a 2-stage process: Initial copper loading forming a “green” T1Cu centre which then undergoes an intramolecular transition to form the final “blue” T1Cu centre. However more research is required to understand the role of the T2Cu site and trimerisation in this process.

Table of Contents

List of abbreviations.

BCS = Bathocuproine disulfonic acid

HOMO = Highest occupied molecular orbital

LUMO = Lowest unoccupied molecular orbital

ROS = Reactive oxygen species

DP-1 = Dansyl peptide 1

DP-2 = Dansyl peptide 2

DP-3 = Dansyl peptide 3

EDTA = Ethylenediaminetetraacetic acid

EGTA = Ethylene-bis(oxyethylenenitrilo)tetraacetic acid

IPTG = Isopropyl β-D-1-thiogalactopyranoside

LB = Lysogeny broth

NHT = No His tag

Nik = Copper dependent nitrite reductase

NTA = Nitrilotriacetic acid

OD = Optical density

PAR = 4-(2'-Pyridylazo)resorcinol

SUMO = Small Ubiquitin-like Modifier

ΔG = Gibs free energy change

ΔH = Enthalpy Change

ΔS = Entropy Change

Declaration

This thesis was composed by myself, that the work contained herein is my own except where explicitly stated otherwise in the text, and that this work has not been submitted for any other degree or processional qualification except as specified.

Statement of Copyright

The copyright of this thesis rests with the author. No quotation from it should be published without the author's prior written consent and information derived from it should be acknowledged.

Acknowledgements

My deepest thanks must go to Dr Karrera Djoko your patients, kindness, and wise advice have been invaluable in a project that has been testing with many unforeseen difficulties. This project simply would not have reached this point without your enthusiasm and support. Thanks also to Dr Samantha Firth for both setting up such a strong foundation for my work to build on and for all your practical assistance during the beginning of this project. Finally, thanks to Jack Bolton and Beth Kinniment-Williams for the practical assistance and moral support you offered whilst working alongside me throughout this project.

Chapter 1: Introduction

1.1 Metals in biology.

It is estimated that >40% of enzymes possess a transition metal in their active site[1,2]. However, the role of *d*-block transition metal ions, such iron nickel and copper, in biochemistry is often underappreciated. Though these elements make up a negligible percentage of atoms within biological systems, they are essential for biology. *d*-block metal ions have unique chemical properties including biologically accessible HOMO's and LUMO's and variable oxidation states. Such properties, not present in the more abundant non-metallic elements, allow metal-binding proteins to carry out useful reactions. Metal ions can act directly as Lewis acids and bases accepting and donating electrons from other biomolecules [3]. They can also activate their ligands by increasing a mixture of acidity, nucleophilicity or electrophilicity [4]. These properties give metalloenzymes a novel set of catalytic mechanisms allowing them to catalyse different reactions or reach higher K_{cat} values.

Metalloproteins form when amino-acid residues (usually side chains) acting as metal-binding ligands coordinate the metal ions thereby creating metal-protein complexes. Nitrogen, oxygen and sulfur atoms in amino acids can coordinate metal ions by can acting as Lewis bases donating electrons to the metal centre, this is often aided by prior deprotonation [5]. As multiple amino-acid side chains from one protein can bind the same metal this allows proteins to take advantage of the chelation effect. Here multi-dentate ligands benefit from a smaller decrease in entropy when compared to mono-dentate ligands giving them a stronger binding affinity. With this strong binding affinity proteins are highly capable of binding a large range of metals.

This however create the issue of mismetalation where non-cognate metals bind incorrectly to proteins disrupting their structure and function [6,7]. This is particularly problematic as metals which are high in the Irving Williams series [8] have higher binding affinities irrespective of ligand. This is as differences in metals electronic structures mean that complex formation facilitates different electronic stabilisation with high stabilisation energies creating higher affinity complexes. Proteins have attempted to counter this by controlling the size of metal binding sites or matching their ligands to the desired metal using the rules of soft acids and bases [9,10] . These factors can however only provide limited preferability before they start to inhibit protein function [11] and aren't enough to counter the Irving Williams series. As such cells have developed import and efflux pumps to tightly maintain the availability of metals which contracts the effect of the Irving Williams series as shown in Figure 1.1 [12].

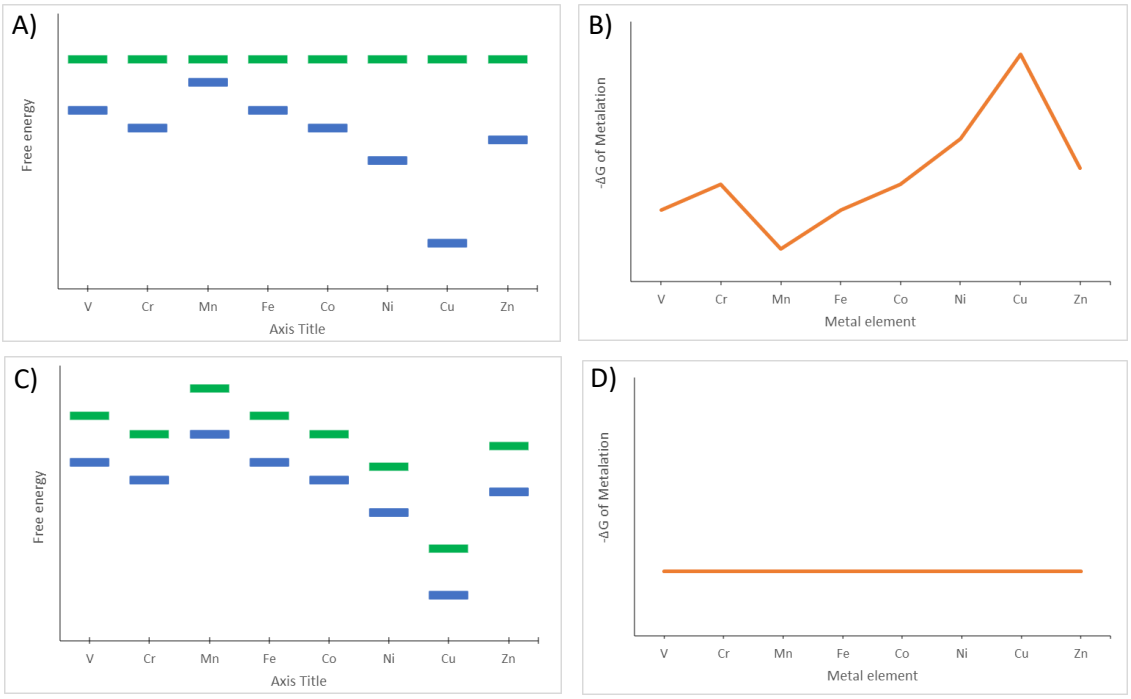

Figure 1.1: Graphic representation of how cells overcome the Irving Williams series. **A)** This shows the free energy of both buffered (---) and protein bound (---) metals in a theoretical cell with no homeostatic control over metal free energies and **B)** shows the free energies of metalations that would result from this with Copper being the most favourable. **C)** Shows the free energy of both buffered (---) and protein bound (---) metals in a real cells with homeostatic control over metal free energies and **D)** shows how this results in a situation where no metal is inherently favoured.

Alongside this homeostatic control of the availability of metals within cells more directed intracellular metal trafficking pathways also exist. These pathways use metal-binding proteins called metallochaperones [13,14] which bind cellular metals and help deliver them into cognate destination protein. Several mechanisms for process have been put forward but most assume some form of transient protein-protein interactions [15] . The exact reason for metallochaperones is also not fully understood but may include increased metal specificity [16], reducing the quantity of free cytosolic metals [17] and acting as insertases by lowering the energy barrier of metalation reactions [18] . But what is known is that mutations in these proteins can have catastrophic impacts on metal trafficking in cells leading to cell death [19]. Understanding the function of these metallochaperones therefore has multiple real world use cases. It can help to develop cures for diseases and is a potential target for new antimicrobials.

1.2 Copper in biology

Copper presents perhaps the greatest challenge in metal trafficking for all cells. Its position towards the right of the transition metals means it has most valance electrons of the first-row transitions metals meaning it benefits from the highest electronic stabilisation energies. Cu (II) also has a d9 electronic configuration meaning copper complexes are electronically stabilised by the Jahn-teller effect [20] mean it has the highest binding affinity in the Irving Williams series.

Copper is a key nutrient within cells. 2.4 billion years ago during the evolution of early life forms oxygenic photosynthetic cyanobacteria caused an increase in the percentage of molecular oxygen in the atmosphere [21]. This simultaneously reduced the availability of iron, which precipitated out of the oceans as insoluble Fe(III) salts, and increased the availability of copper as insoluble Cu (I) salts were oxidised to form the more soluble Cu (II) salts [22]. The combination of these processes are thought to have led to the eventual incorporation of copper into key enzymes, such as those in the respiratory[23].

Handling of copper by cells is a careful balancing act because sufficient copper must be available for the function of copper- dependent metalloenzymes (cuproenzymes) but not to much because it is potentially toxic. Like other metal ions, when is present at toxic quantities it can mismetalate non-cognate metal-binding sites in metalloproteins or binding adventitiously to amino acids in non-metal binding proteins. One example of this is the mis metalation and subsequent inactivation of fumarase A in *E. coli* by excess copper ions which displace iron in the Fe-S clusters found in the fumarase active site [24]. Excess copper can also damage cells by catalysing the production of hydroxyl radicals and other reactive oxygen species (ROS) a fenton-like mechanism as shown in equations 1a and 1b [25].

Eq.1.1a $$Cu^{2+} + H_2O_2 \rightarrow Cu^{+} + 2H^{+} + 2\,O^{-\cdot}$$

Eq.1.1b $$Cu^{+} + H_2O_2 \rightarrow Cu^{2+} + OH^{\cdot} + OH^{-}$$

Hydrogen peroxide an unwanted byproduct of oxygenic respiration and is therefore ubiquitous in obligate and facultative aerobes [26]. In these cells copper can therefore create large quantities of ROS which cause oxidative stress by oxidising with amino acids [27] , DNA [28] and lipids [29]. These can affect metabolism and can lead to cell death particularly when DNA is damaged.

To mitigate these risks organisms have evolved a series of classes of proteins including, regulators, import and export pumps and metallochaperones [30,31]. One system that demonstrates how these proteins function is the cop-operon found many gram-positive bacteria including *Enterococcus*

hirae[32]. The operon contains 4 genes: copA, cop B, copY and copZ. CopZ is a metallochaperone which, when excess cellular copper is present, delivers copper into copY displacing zinc from a metal-binding site [33]. CopY is a zinc-dependent transcriptional repressor [34] and the binding of copper therefore causes it to release the DNA. This leads to transcription and translation of cop A and copB which are ATP-driven pumps with that export the excess copper [35,36]. Due to its high binding affinity copper is maintained at a very low concentration within cells which is often achievable through simple diffusion. Copper import pumps are therefore less common that export pumps for other metals. However, examples of import pumps are found in metal-sensitive bacterial strains such as *Bacillus subtilis* [37].

All these different copper binding proteins use similar amino acid residues to form ligand bonds with copper and this allows copper binding sites to be categorised as is shown in table 1. Coppers low charge makes it the softest of the commonly bioactive metals. This limits the amino acids that it can bind to Cystine and Methionine, which are considered softer due to the large atomic radii of sulphur, or Histidine and Glutamate, which are softer due to the delocalised nature of their negative charge.

Table 1.1: Metal centres formed by copper [38,39].

Centre	Number of Copper atoms	Geometry	Coordination
T1 (Class I)	1	Tetrahedral	2x N_{His}, S_{Cys} and S_{Met}
T1 (Class II)	1	Tetrahedral	2x N_{His}, S_{Cys} and O_{Glu}
T1 (Class III)	1	Trigonal Bipyramidal	2x N_{His}, $S_{Cys,}$ S_{Met} and O_{Glu}
T2	1	Square Pyramidal	4x N_{His} and H_2O
T3	2	Trigonal Bipyramidal	3xN_{His} and Bidentate O_2 bridging ligand
Cu_A	2	Tetrahedral	2 Cu centres: Cu1 = N_{His}, O_{Glu} and 2x bridging S_{cys} , Cu2 = N_{His}, S_{Met} and 2x bridging S_{cys}
Cu_Z	4	Distorted Tetrahedron	Inorganic Sulphur and 7xN_{His}
Cu_B	1	Trigonal pyramidal	3xN_{His}
Cu_C	4	Tetrahedron	No yet well characterised

1.3 The role of copper-dependent nitrite reductase AniA in Neisseria gonorrhoeae.

One class of enzymes that act as of a key respiratory cuproenzyme is the copper dependent nitrite reductases (Nik). Alongside Fe-containing nitrite reductases these enzymes catalyse the first committed step of denitrification pathway [40]. This pathway uses terminal electrons produced by respiration to break down nitrite into Nitrogen gas in the 3 steps process shown in equations 2a, 2b and 2c below. This is environmentally critical as it closes the nitrogen cycle and is involved in many of the issues created by the use of artificial fertilisers. It is also important in the study of many pathogens as the process allows them to survive in oxygen limited environments [41].

Eq. 1.2a $$NO_2^- + e^- + 2H^+ \rightarrow NO + H_2O$$

Eq. 1.2b $$2NO + 2e^- + 2H^+ \rightarrow N_2O + H_2O$$

Eq. 1.2c $$N_2O + 2e^- + 2H^+ \rightarrow N_2 + H_2O$$

One such pathogen is *Neisseria gonorrhoea* which contains the Nik AniA. *N. gonorrhoea* is a Gram-negative, obligate human pathogen which causes 86.9 million infections globally [42.] The denitrification pathway allows *N. gonorrhoea* to respire in the absence of oxygen [43,44] using nitrite as the terminal electron acceptor. This process is important for gonococcal pathogenesis since anaerobic growth is strongly associated with biofilm which facilitates gonococcal colonisation and survival in the human genitourinary tract [45,46].

In *N. gonorrhoeae*; the denitrification pathway is truncated. Initially AniA reduces nitrite with the addition of one electron to form nitric oxide [47] (Equation 1.2a). This nitric oxide is then further reduced by the heme-dependent enzyme NorB, forming nitrous oxide [48] (Equation1.2b). While the genes for a copper-dependent nitrous oxide reductase that reduces nitrous oxide to dinitrogen gas are present this enzyme is functionally absent in *N. gonorrhoea* due to the presence of a premature stop codon[49].

AniA is known to be expressed during *N. gonorrhoeae* pathogenesis in the human host since the protein is targeted by antibodies found in human sera [50]. Understanding the function of AniA is therefore of a broad interest as it represents a potential target for new anti-biotics [51] , a pressing issue given the global rise of antibiotic resistant strains of *N. gonorrhoeae* [52,53].

1.4 The structure and function of AniA.

The enzyme AniA is a functional homotrimer containing a total of 6 copper binding sites, of which 3 are T1 copper and 3 are T2 copper [54]. In the T1 site (Figure 1.2b), the copper ion is bound by 4 amino acid residues, all of which come from the same polypeptide: cys-175, met-188, his-134 and his-183. In contrast the T2 site (Figure 1.2e) exists on the trimer interface and binds copper with his-139 and his-174 from one peptide and his-329 from a neighbouring polypeptide.

The T1 copper in Nik's acts as the site of electron entry from a donor partner which is thought to be C_n and CcoP c-type cytochromes[55]. The reduced T1 copper then transfers its electron through a Cys-His bridge[56] (Figure 1.2c) to the T2 copper. The T2 copper in its reduced Cu(I) state is then used to reduce the nitrite into nitric oxide (Figure 1.2d)[57].

The AniA is also known to be tethered to the outer membrane of *N. gonorrhoea* by a bond which forms between an N-terminal Cystine residue and a palmitate residue [58]. This location explains why it is targeted by human antibodies. Analysis of AniA proteins from a range of species show that it is likely transported across the inner-membrane by the sec pathway. This means that it is folded and metalated in the periplasm [59].

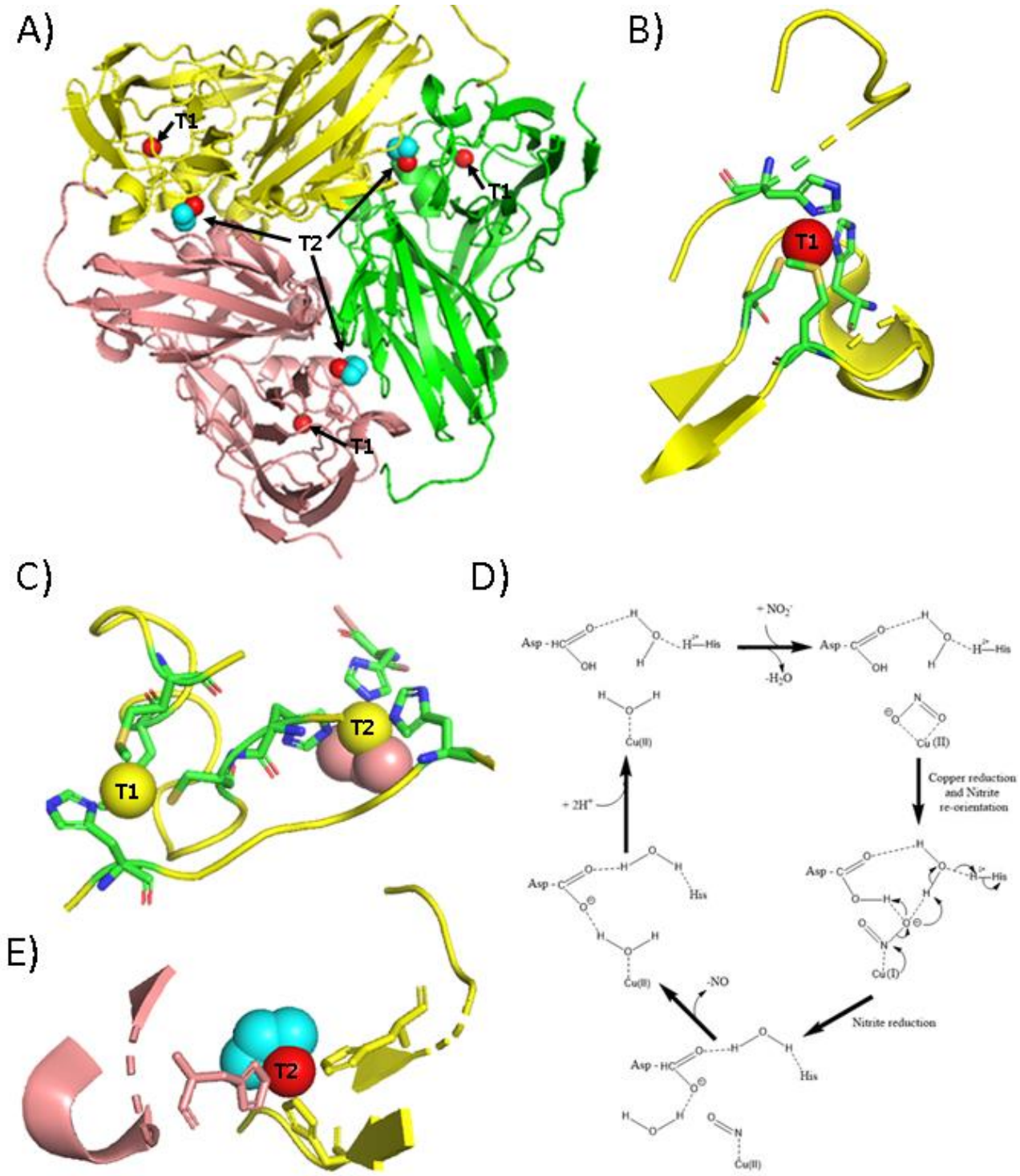

Figure 1.2: 3D structure of AniA. **A)** This shows entire structure of the Active Holo-AniA trimer. **B)** This shows the structure of the T1 site with copper binding amino acids: cys-175, met-188, his-134 and his-183. **C)** This shows the relative positions of the T1 and T2 site and how they are connected by the Cys-His bridge. **D)** This is the mechanism of catalytic nitrite reduction that occurs at the T2 copper in AniA. **E)** This is the structure of the T2 site showing how it binds histidine residues his-139 and his-174 from one peptide and his-329 from a second polypeptides. [54,57,60].

1.5 Copper insertion into AniA

As discussed above the management of copper within cells is often complicated and AniA is no different. The predicted secretion of AniA into the periplasm as an unfolded polypeptide via the Sec translocon has raised the question of how this protein acquires copper. Mutagenic studies revealed that a secondary periplasmic protein, later named AccA, was involved in the function of AniA in *N gonorrhoeae* [61]. When AccA was knocked out AniA polypeptide was produced but was not active. Initial biochemical analysis of AccA showed it was homologous to the PCu_AC family of metallochaperones which are thought to assist the formation of haem-Cu oxidases [62]. AccA shares a conserved contains a high-affinity Cu(I) binding site with the PCu_AC family of metallochaperones. It also contains a low-affinity Cu(II binding site in the C-terminus [59,63]. Further work has also shown *in vitro* transfer of copper from AccA to AniA further indicating that AccA acts as a metallochaperone.

However, the mechanism of copper transfer between AccA and AniA is yet to be elucidated. The key challenge is how to track the presence or absence of copper in either protein. The most convenient method of tracking Cu-insertion is UV-vis spectrophotometry. This is as many metal complexes absorb light in the visible range. The energy from the light which is absorbed excites electrons to move into higher energy orbitals however the rules of quantum mechanics mean only certain energy transitions are allowed. These broadly split into 2 categories: d-d transitions and charge transfer. D-d transitions occur when electrons move between d orbitals within the metal ion itself, these are Laporte forbidden and therefore tend to have weaker extinction coefficients. In contrast Charge transfer transitions occur in complexes containing π bonds and see electrons transfer from the p-orbitals of ligands to the d orbitals of the metals. They are therefore allowed by the Laporte rule and therefore have stronger extinction coefficients.

Cu (I) with its d10 electron configuration does not have any accessible orbitals and all Cu (I) centres are therefore spectroscopically silent. Histidine residues bond through σ-bonds and therefore do not have any charge transfer transitions, this means all T2 sites are spectroscopically silent. T1 sites do however have a charge transfer band due to the Cu(II)-cys bond. In AniA this results in a characteristic absorbance with a minor band at 460nm and a major band at 600 nm.

Another challenge in understanding the metalation of AniA is that insertion of copper appears to be associated with trimerisation. Recent work from Dr S Firth showed that purified apo-AniA is a monomer in solution. Upon incubation with copper this protein undergoes trimerization. This is not entirely surprising as crystal structures show the T2 copper is coordinated by ligands from two different polypetides[59].

This does leave many questions still to be answered: Is AccA a metal dependent catalyst for the metalation of AniA? What is the relationship between metalation and trimerization? In what order do binding sites acquire copper from AccA? What is the structure of any intermediates? However, to answer these questions several experimental advances are required. Firstly a structure of apo-AniA is needed which requires a high purity sample of AniA. Secondly methods are required to track the presence or absence of copper in all major binding sites.

1.6 Project aims.

The primary aim of this project is to understand the mechanism of metalation of AniA in *Neisseria gonorrhoea.* Though the final aim is to understand the *in vivo* transfer of copper from holo-AccA to apo-AniA so little is known about both proteins that this project will start by attempting to better understand *in vitro* metalation of Apo-AniA from an aqueous inorganic source of copper. The expectation is that new understanding and tools developed during this project can then be used to better understand the system *in vivo*.

The starting point of this project therefore has four key aims: Purify a pure sample of apo-AniA for structural analysis, develop tools to track the metalation of the spectroscopically silent T2 copper binding site, measure the affinities of both the T1 and T2 binding sites and thirdly better understand the relationship between metalation and trimerization.

Chapter 2: Materials and Methods

2.1 Preparation and transformation of chemically competent cells

To prepare chemically competent cells *E. coli* strains were grown overnight on LB agar plates containing the appropriate antibiotic (Table 2.1). Cells where then grown on in 100 ml of LB broth (Melfords) in a shaking incubator (37°C, 180rpm) until they reached OD = 0.4. At this point the cells were cooled on ice for 20 minutes then centrifuged at 4 °C, 4000rpm for 10 minutes. The supernatant was discarded and the pellet was resuspended in 20 mL of ice-cold 01.M $CaCl_2$. Cells were incubated on ice in this solution for 30 minutes then centrifuged again at 4 °C, 4000rpm for 10 minutes. The supernatant was again discarded and the cells in the pellet where resuspended and frozen in 5ml of ice-cooled 0.1M $CaCl_2$ with 15% glycerol.

Chemically competent cells were transformed using the heat shock method. Frozen stocks where first thawed on ice, 2 µL of purified plasmid DNA or 10 µL of ligation mix was then added and mixed carefully. Cells where then incubated on ice for 60 minutes then heat shocked for 50 seconds at 42°C before a further 5 minutes of incubation on ice. 900 µL of LB broth was then added and the cells were incubated for 3 hours (37°C, 180rpm). Cells where then centrifuged at 13,000 RPM for 1 minute, the supernatant was discarded, and the pellet was resuspended in 100 µL of LB broth. 50 µL of this inoculated broth was then spread on sterile LB agar plates containing the appropriate antibiotic (Table 2.1) to select for successful transformation. The plates were grown overnight and colonies where then propagated on fresh plates before being stored at -60°C in LB broth containing 20 w/v % glycerol.

2.2 *E. coli* growth conditions and strains.

The *E. coli* strains used in this study (Table 2.1) were stocked in LB broth (Melfords) with containing 20 w/v % glycerol and stored at -80 ^{o}C. When needed, *E. coli* strains were propagated from glycerol stocks on LB agar (Melford) which contained the appropriate antibiotic (Table 2.1). The bacteria were incubated overnight at 37 ^{o}C, after which they were harvested and used for downstream processes.

Table 2.1: List of *E. coli* strains used in this study.

Strain	Use	Antibiotic resistance
DH5α	Plasmid Propagation	-
BL21 Rossetta pLySs	Protein Overexpression	Chloramphenicol
BL21 Rossetta 2	Protein Overexpression	Chloramphenicol
BL21 Codon Plus(+)	Protein Overexpression	Chloramphenicol

Table 2.2: List of antibiotics used during bacterial growth.

Antibiotic	Concentration (μg/mL)
Ampicillin	100
Chloramphenicol	30
Kanamycin	100

2.3 Generation of AniA overexpression constructs.

All new overexpression constructs AniA used in this study were generated by altering the pET29a: AniA TC plasmids which was sourced from Dr Samantha Firth[59]. Changes to the plasmid were made using PCR reactions involving overhanging primers that introduced the changes and B*sa*I restriction sites (Table 2.3). PCR reaction used Q5 DNA polymerase (New England Biolabs) following the manufactures protocol. The resulting linear PCR products were digested with BsaI-HF v2 restriction enzyme (New England Biolabs) and re-circularised using a T4 DNA ligase (New England Biolabs). The resulting constructs were transformed into chemically competent *E. coli* DH5α cells for propagation. The final plasmid was extracted out of the DH5α cells using a Monarch Plasmid Miniprep Kit (New England Biolabs). All DNA fragments produced during this process where initially tested for purity and length using agarose gels. DNA was stained with SyBr (Invitrogen) and compared to a 1kB ladder (New England Biolabs). The sequences of all overexpression constructs were confirmed *via* Sanger sequencing at Durham Universities Genomics facility.

Table 2.3: List of primers used in this study.

Construct Name	**Template**	**Primer Name**	**Primer Sequence (5'->3').** (Cleaved region will be in red and Overhang sequence will be in blue)
NHT-AniA	pET29a-TC-AniA	AniA-HisRem-F	ATTAGCTGGTCTCACGTATGAGATCCGGCTGCT
		AniA-HisRem-R	ATATATCGATGGTCTCATACGGCGTAAGCGGTATC
C-term 3c AniA	pET29a-TC-AniA	AniA C-Term 3c ins F	ATATAGGTCTCATGTTCCAAGGTCCTAGCCTCGAGCACCACCACCAC
		AniA C-Term 3c ins R	GCGCGGTCTCGAACAATACTTCCAAGGCGTAAGCGGTATCACTCAATT
N-term 3c AniA	pET29a-NHT-AniA	AniA N-Term 3c ins F	ATATATGGTCTCATGGAAGTATTGTTCCAAGGTCCTGCCGCACAAGCTACCGCCGA
		AniA N-Term 3c ins R	GCGCGGTCTCATCCAATCGTGCTGCGTGGTGGTGGTGGTGGTGCATATGTATATCTCCTTCTTAAAGTTAAAC

Table 2.4: List of plasmids used and generated in this study.

Plasmid name	**Description**	**Source**	**Strain Stocked**
Vectors			
pET29a	Over-expression vector with kanamycin resistance gene.	N. Robinson Lab (Durham)	*E. coli* DH5α
Overexpression			
pET29a: *aniA TC*	Plasmid for overexpression of AniA with a C-terminal 6xHis purification tag connected by a thrombin cleavage site.	Sam Firth	*E. coli* BL21 pLySs
pET29a: *aniA NHT*	Plasmid for overexpression of AniA containing no purification tag	This Work	*E. coli* BL21 Rossetta 2
pET29a: *aniA SUMO*	Plasmid for overexpression of AniA with an N-terminal 6xHis-SUMO tag.	Karrera Djoko & this work	*E. coli* BL21 Rossetta 2
pET29a: *aniA 3C*	Plasmid for overexpression of AniA with a C-terminal 6xHis purification tag connected by a 3C protease cleavage site.	This Work	*E. coli* BL21 PLySs

2.4 Protein overexpression and purification.

Table 2.5: Buffers used during protein purification.

Buffer name.	Buffer contents.
Resuspension Buffer A	50 mM Tris-HCl pH 8.0, 150 mM NaCl, 5 mM imidazole, 15% glycerol
Resuspension Buffer B	50 mM Tris-HCl pH 8.0, 150 mM NaCl, 15% glycerol
General W0	50 mM Tris-HCl pH 8.0
HisTrap W5	50 mM Tris-HCl pH 8.0, 5 mM imidazole
HisTrap W25	50 mM Tris-HCl pH 8.0, 25 mM imidazole
HisTrap E250	50 mM Tris-HCl pH 8.0, 250 mM imidazole
Q-Column E250	50 mM Tris-HCl pH 8.0, 250 mM NaCl, 15% glycerol

2.4.1 Overexpression of AniA variants

Having been propagated overnight on LB agar plates containing kanamycin and chloramphenicol, *E. coli* BL21 cells carrying the different pET29a constructs were resuspended in 1x PBS. They were subsequently used to inoculate baffled 2 L flasks, each containing 1 L of LB broth (Melfords), kanamycin and chloramphenicol, to a final OD_{600} of 0.01. These cultures were then grown for an initial period at 37 ^{o}C with shaking at 180 rpm for ~4 hours until OD_{600} > 0.4. At this point, protein expression was induced by adding IPTG (Isopropyl β-D-1- thiogalactopyranoside) to a final concentration of 0.1 mM as all overexpression constructs used in this study were induced by a T7 promotor. The cultures were further supplemented with kanamycin to maintain the plasmid. These cultures where cooled to 22 ^{o}C and grown for an additional 4 hours until they were centrifuged (6000 rpm, 4 °C, 15 minutes) using an Avanti J26-XP centrifuge with a JLA-16.250 rotor (Beckman-Coultier).

Following centrifugation, the spent culture supernatant was discarded and the pellets were resuspended. NHT-AniA pellets were resuspended in Resuspension buffer A whilst other variants were resuspended in Resuspension buffer B (Table 2.5). Bacteria were then lysed by sonication using a Q700CA sonicator (Thermo Scientific). Sonication took place for a total of 7 minutes, split into 21 cycles of 20 s “ON” followed by 20s “OFF” with continuous cooling by ice bath. Following lysis, cell debris was removed by 2 rounds of centrifugation with a JA 25:50 rotor (21000 rpm, 4 °C, 30 minutes each). After each round of centrifugation, the cell lysate supernatant was kept whilst the debris was discarded. Any remaining debris in the supernatant was filtered out using 0.45 µm polyethersulfone syringe-driven filter units (Starlab).

2.4.2 Purification of AniA proteins

Filtered cell lysate supernatants were loaded onto 5 mL HisTrap™ columns (Cytiva) that had been pre-equilibrated General buffer W0 (Table 2.5). The column was washed with His-trap W25 (Table 2.5) until no more protein was eluted, as detected by solution absorbance at 280 nm, which usually required around 25 column volumes. To elute bound proteins, 5 mL Q-HP columns (Cytiva) were connected to the bottom of the HisTrap columns and the protein was eluted directly from the HisTrap columns onto the Q columns using 15 ml of HisTrap E250 buffer (Table 2.5). Next, the HisTrap columns were disconnected and the Q columns were washed with General W0 buffer (Table 2.5) until no more protein was eluted. Finally, bound proteins were eluted from the Q columns using Q-column E250 buffer (Table 2.5). Eluents were collected in 1.5 mL tubes and fractions with the highest possible protein concentrations were kept and used for further experiments. All purification steps were carried out at room temperature and with a flowrate of 1-2.5 mL/min.

During purification all fractions were collected mixed with Bromophenol SDS loading dye and run on a Bis-Tris SurePAGE gels (Genscript) in a pH 7.0 Tris-Mops Buffer. Gels where then stained with a Coomassie Blue stain (NeoBiotech).

2.4.3 Cleavage conditions

When AniA samples required thrombin cleavage they were eluted from the Q-column using 2xPBS. This was then diluted to a concentration of 1xPBS. Thrombin (Cytiva) was then added and samples were incubated overnight at 22°C.

AniA samples requiring 3C cleavage were cleaved in Tris buffer at pH 8.0 in a solution containing 1mM Dithiothreitol. 3C protease (Dr Liz Morris, Durham University) concentrations where 7.5 mg/ml and the reaction was carried out overnight at 4°C.

2.4.4 Measuring protein concentrations.

Protein concentration in a sample was estimated using UV-vis spectrometry by to measuring the absorbance of the sample at 280 nm. This absorbance was then converted to protein concentration using Beer-Lambert's law (Equation 2.1) and a predicted extinction coefficient (ε) for AniA of 24870 cm^{-1} M^{-1}. This extinction coefficient was obtained using the ExPASy ProtParam tool using the reported amino acid sequence of AniA.

Eq.2.1 $$A = \varepsilon c l$$

2.4.5 Verification of purified *apo*-AniA proteins.

The molecular mass of all purified proteins was confirmed via Electrospray Ionisation Mass Spectrometry in the positive ion mode at the Mass Spectrometry Facility, Department of Chemistry, Durham University. The results of this can be seen in table 2.6

Table 2.6: Theoretical and actual masses of proteins purified during this study.

Protein	Theoretical Mass(kDa)	Actual Mass (kDa)
AniA – thrombin -His	36.241	36.222
AniA (cleaved)	35.014	35.012
ΔT2 AniA	34.463	34.465

When more information was required about the sequence of unknown protein fragments these proteins where sent for MALDI-TOF peptide analysis at the Proteomics Facility, Department of biosciences, Durham University.

The metal content of AniA was also measured by reacting samples with 4-(2'-Pyridylazo)resorcinol (PAR). The AniA samples where denaturation using Guanidinium chloride to release any bound copper which could then bind PAR. The results where then compared with a standard Copper vs PAR curve showing that purified AniA samples where effectively copper free.

2.5 Preparation and calibration of metal and probe stock solutions.

Stock solutions of $CuCl_2$ were prepared by dissolving $CuCl_2$ solids in deionised water. Their concentrations were determined using excess solutions of bathocuproine disulfonic acid (BCS) which binds Cu(I) and acts as a colorimetric reporter.

Eq.2.1 $$2\,BCS + Cu(I) \rightleftharpoons Cu^{I}(BCS)_2$$

To do this, a stock solution of BCS was prepared in 50 mM MOPS buffer pH 7.2 to a concentration of >1 mM. This BCS stock was then added to a known volume of a working stock solution of $CuCl_2$, along with 2 mM of sodium ascorbate. Sodium ascorbate reduced Cu(II) to Cu(I), which in turn became chelated by BCS (Eq. 2.1). Given the large excess of both BCS and sodium ascorbate, it can be assumed that all copper in solution was reduced and bound by BCS. As the $[Cu^{I}(BCS)^{2}]^{3-}$ anion has

a characteristic absorbance at 483 nm with a known extinction coefficient of 1300 $M^{-1} cm^{-1}$, this allows the concentration of copper in the original $CuCl_2$ stock solution to be determined accurately.

2.6 Measuring Cu insertion into AniA proteins.

Copper loading experiments, both endpoint and kinetic, where performed in 50 mM Tris pH 7.4 with AniA concentrations of either75 µM unless otherwise stated. All experiments also recorded the entire spectra of AniA from 250 nm – 800 nm.

Endpoint experiments were carried out in 1.5 mL tubes. Samples where then loaded into cuvettes (Eppendorf) and measured in a blanked UV-vis spectrometer. For experiments with a competitor ligand the competitor ligand had a concentration of 225 µM to ensure it was always in excess compared to copper.

Kinetic experiments carried out in UV-Star® 96-well microplate (Grainer) with reading taken on a SPECTROstar nano plate reader (BGM Labtech). Initial reading were taken without the addition of copper to measure a stable blank then upon the addition of copper reading were taken every 30s.

2.7 Measurement of protein fluorescence.

Measurements were carried out on a Jobin–Yvon Fluoralog-3 fluorimeter. Fluorometry work used the same samples which had been created for endpoint kinetic experiments. Samples were diluted with 50 mM tris pH 7.4 to a protein concentration of 4 µM and placed in 3 mL crystal cuvettes. Various excitation and emission spectra were taken to find the optimal sensitivity and exposure settings for clear results before recording experimental results.

Chapter 3: Overexpression of AniA

The eventual plan for this project was to examine Cu insertion into *apo*-AniA and trimerization, and to determine the structure of *apo*-AniA, which is currently unknown. No structure of *apo*-NirK has been reported in the literature. This plan requires high quantities of *apo*-AniA in high purity.

Previous studies of AniA in our lab and elsewhere [54,59] employed an overexpression construct in which a thrombin-cleavable hexa-His tag is attached to the C-terminus of AniA. This allowed efficient purification of the protein on a Ni affinity column. The hexa-His tag was then removed using a thrombin protease (more detail in section 2.4). Therefore, this was the approach employed in this work. However, mass spectroscopy of the final purified protein (Figure 3.1A) showed three peaks corresponding to the uncleaved AniA protein carrying the hexa-His tag (36221 Da), the desired full-length AniA protein without the hexa-His tag (35011 Da), and a truncated form AniA protein (31381 Da). The mass of the truncated product corresponds to an AniA protein that lacks the last 33 amino acid residues at the C-terminus. We hypothesised that this truncated product was produced by non-specific cleavage between residues Arg292 and Ala293 by thrombin. Unfortunately, this truncated product had similar size and pI to the desired, full-length AniA protein, and therefore could not be separated by standard protein purification techniques.

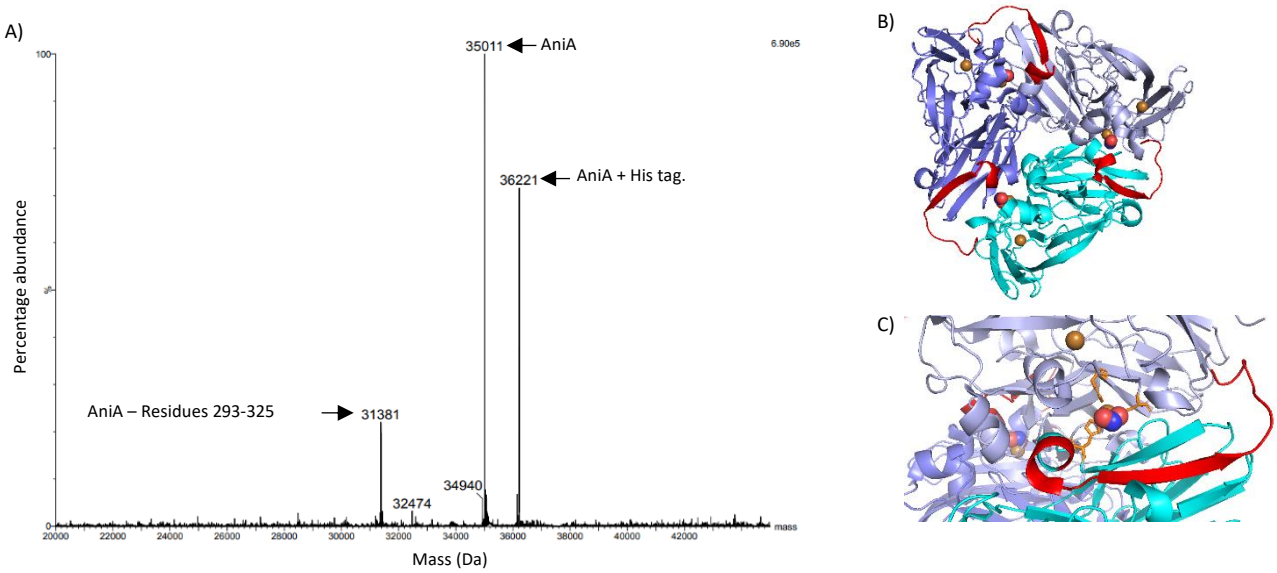

Figure 3.1: A) Mass spectroscopy showing presence of impurities in AniA prepared by thrombin cleavage. **B and C)** Crystal structure showing the region of AniA cleaved non-specifically by thrombin in red[54,60].

In an attempt to eliminate this non-specific cleavage we experimented with reducing the units of thrombin added. Though reducing the units of thrombin did reduce the quantity truncated AniA produced it wasn't able to eliminate it (Figure 3.2). Incubation with 2.5 units of thrombin led to only a small proportion of truncated protein. This form of the protein was deemed suitable for initial examination of Cu insertion into AniA (described in Chapter 4).

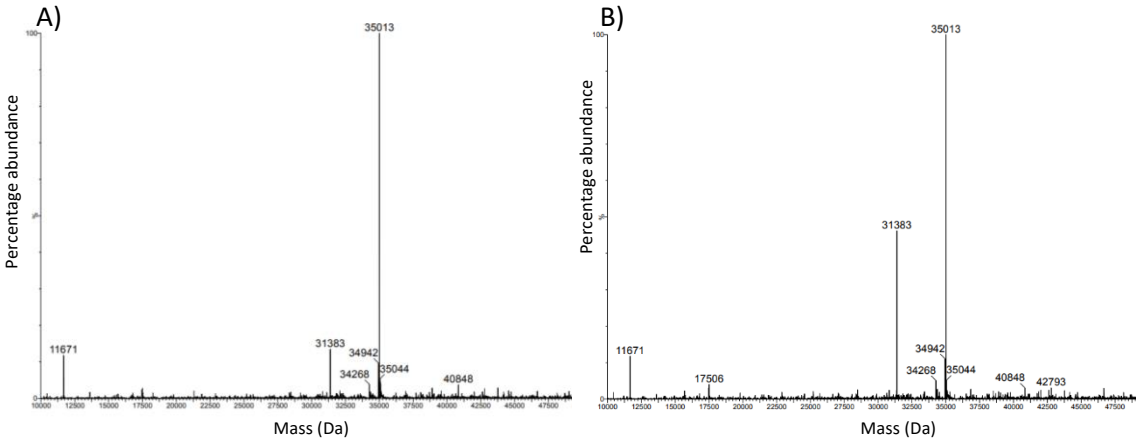

Figure 3.2: Mass spec of AniA-thrombin-His cleavage product when cleaved with **A)** 2.5 and **B)** 12.5 units of thrombin.

It is important to note that the truncation may impact Cu binding and/or trimerization by AniA. Although all Cu-binding ligands are retained in the truncated protein, the cleaved region is close to a T2 ligand (His-329). The cleaved region also participates in the monomer-monomer interface in the *holo*-AniA trimer (Figure 3.1B). The presence of two different forms of the enzyme may suppress crystallisation prohibiting the use of X-ray crystallography. Therefore, we sought a new method to overexpress and purify AniA (summarised in Table 3.1)

Table 3.1: List of protein purification techniques trailed for purification of AniA.

Technique	Tag	Protease	Cleavage recognition sequence
AniA-thrombin-His	C-terminal 6xHis	Thrombin	LVPR/GS
NHT-AniA	-	-	-
His-SUMO-AniA	N-terminal 6xHis	Sumo	(Sumo domain) GG/XX
AniA-3c-His	C-terminal 6xHis	3c	LEVLFQ/GP
His-3c-AniA	N-terminal 6xHis	3c	LEVLFQ/GP

3.1 NHT(No His Tag)-AniA

The first method that we attempted was to remove the hexa-His tag from the overexpression construct to generate NHT-AniA protein. The most effective way of purifying any protein is to separate this protein based on unique protein properties. Unfortunately, AniA is not unusual in its predicted size, pI, or hydrophobicity. However, while investigating the thrombin cleavage method, there were hints that some full-length AniA protein lacking the hexa-His tag bound to the Ni column. The hypothesis here was that the His ligands *apo*-AniA may act as a "natural" His-tag that will bind to a Ni column.

Overexpression tests showed that the target NHT-AniA protein was expressed in Rossetta pLySs when induced with IPTG, as evidenced by the presence of a band between 34 and 43 kDa. However, this protein did not appear to bind to the Ni column, as evidenced by SDS-PAGE gels of the various fractions (Figure 3.3). Instead, it appeared that most of the target protein remained in the flowthrough fraction. To enhance binding of NHT-AniA to the Ni column, we removed imidazole from the initial loading and washing buffers to minimise potential competition. We also increased the pH of these buffers from pH 8.0 up to pH 10.0 to deprotonate the His residues in NHT-AniA and increase their affinities to the Ni column. However, neither of these approaches improved binding of NHT-AniA to the Ni column. The lack of imidazole in the column loading and washing steps also meant that many more contaminating proteins were bound non-specifically to the column, which would complicate downstream purification steps. Therefore, this approach was not pursued further.

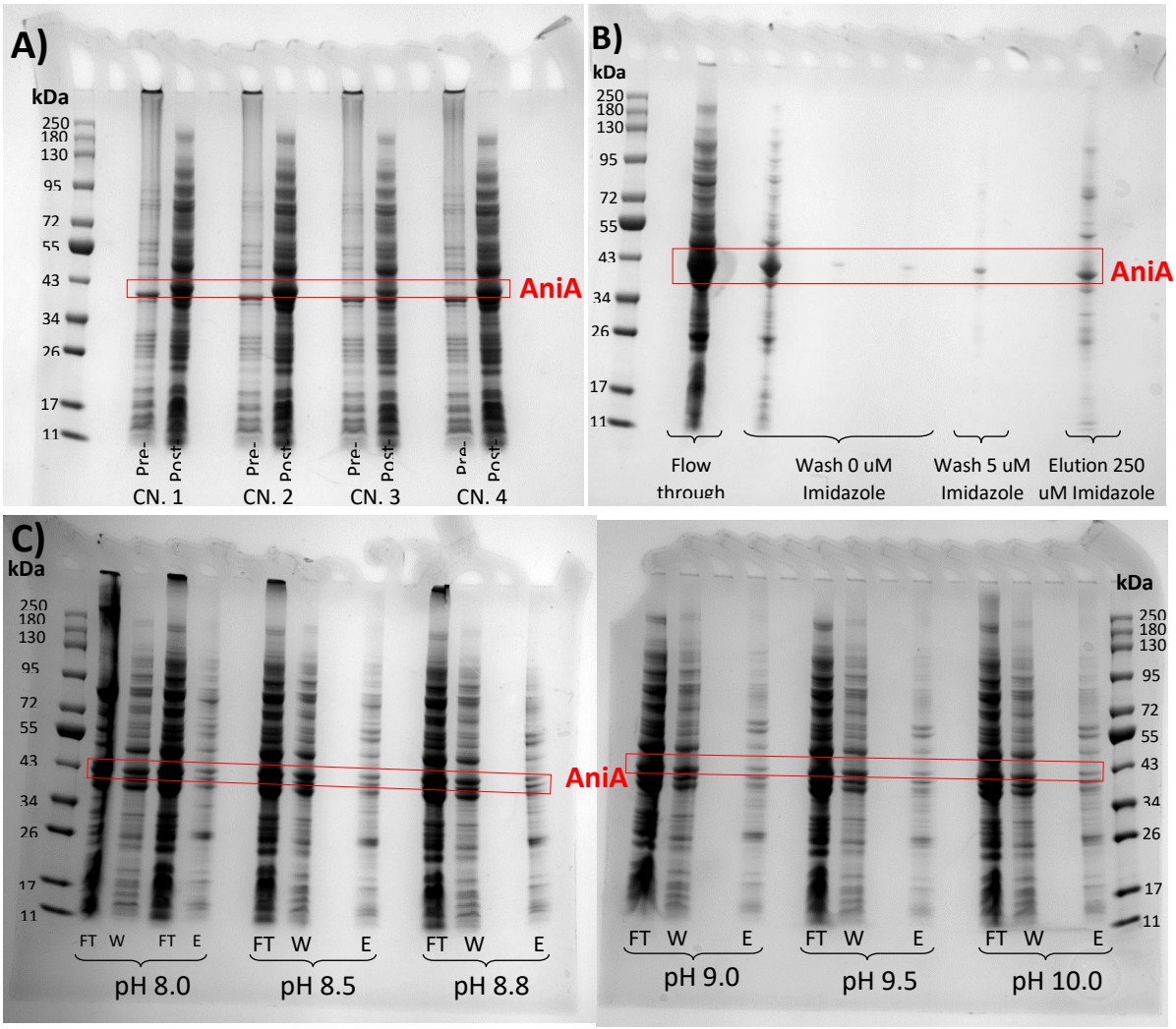

Figures 3.3. Protein gel showing **A)** overexpression of NHT-AniA pre and post ITPG in several colonies of Rosetta pLySs (CN.=Colony Number), **B)** Initial His-trap purification attempt of NHT-AniA and **C)** Trial His-trap purifications of NHT-AniA with varied pH.

3.2 His-SUMO-AniA

The second approach was to introduce a hexa-His- SUMO (Small Ubiquitin-like Modifier) tag at the N-terminus, which can be cleaved by the SENP protease. This approached was employed to produce the wild-type AniA protein, a variant AniA lacking the T1Cu ligands, and a variant AniA lacking the T2Cu ligands. Interestingly, these proteins were not expressed in the Rosetta pLySs expression host, which was used to express NHT-AniA and AniA-thrombin-His proteins. Instead, the His-SUMO-AniA proteins were expressed in Rossetta 2 and Codon+ hosts (Data displayed is from the ΔT2 KO mutant lacking T2Cu site ligands).

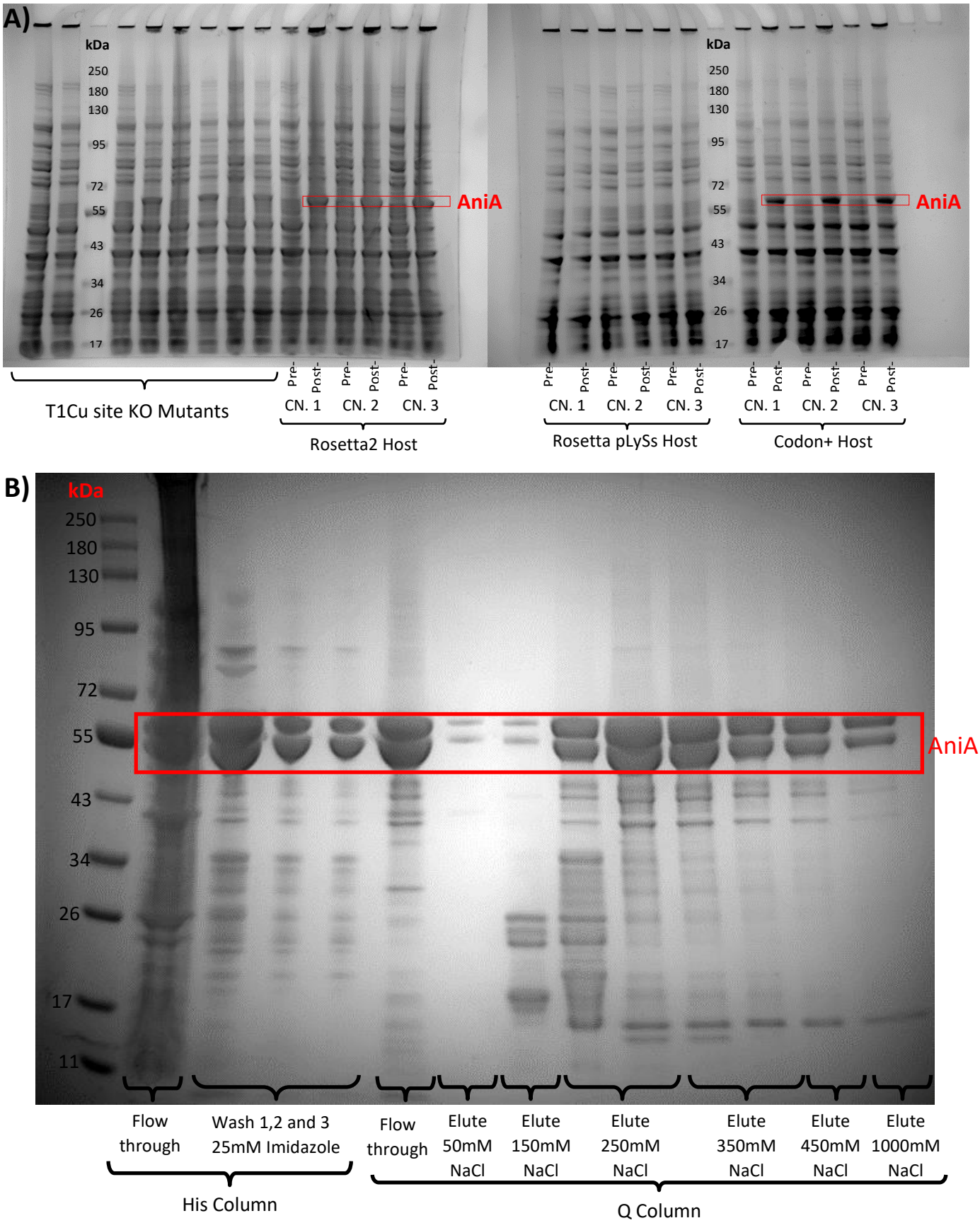

Figure 3.4. Protein gels showing **A)** overexpression of His-Sumo-ΔT2.AniA in different host strains pre and post ITPG induction and **B)** purification of His=SUMO- ΔT2.AniA protein using His and Q column.

Frustratingly, His-SUMO-AniA protein appeared to spontaneously generate the truncated form of AniA, even prior to addition of the protease. This is evidenced by the gel shown in Figure X, which shows two bands centred around 55 kDa. Analysis of the two bands by MALDI-TOF peptide analysis at Durham Biosciences Proteomics Facility confirmed that both bands were AniA. Addition of SENP protease did not appear to truncate the protein any further. The SENP-digested sample, with the His-SUMO domain removed, was then analysed by ESI-MS. The results showed two major bands at of 34465 kDa and 30497 kDa, corresponding to the full-length ΔT2-AniA protein (the variant lacking T2 ligands) and a truncated form lacking 37 amino acids at the C-terminus (highlighted below).

AAQATAETPAGELPVIDAVTTHAPEVPPAIDRDYPAKVRVKMETVEKTMKMDDGVEYRYWTFDGDVPGRMIRVRE
GDTVEVEFSNNPSSTVPHNVDFAAATGQGGGAAATFTAPGRTSTFSFKALQPGLYIYACAVAPVGMHIANGMYGL
ILVEPKEGLPKVDKEFYIVQGDFYTKGKKGAQGLQPFDMDKAVAEQPEYVVFNGHVGAIAGDNALKAKAGETVRM
YVGNGGPNLVSSFHVIGEIFDKVYVEGGKLINENVQSTIVPAGGSAIVEFKVDIPGNYTLVDASIFRAFNKGALG
QLKVEGAENPEIMTQKLSDTAYA

As the two bands were present before addition of SENP, we hypothesised that cleavage was catalysed by an unknown protease in the *E. coli* lysate. It is particularly interesting that this cleavage occurs in a similar protein region, near the non-specific thrombin cleavage site described earlier. It is possible that this region is structurally flexible and thus susceptible to non-specific proteolytic cleavage. In the future, protease inhibitors can be added to the lysis and purification steps.

Looking back, the amount of NHT-AniA in the previous section appeared to decrease with each purification attempt. NHT-AniA may suffer from the same non-specific cleavage, even though the expression host was different. Intriguingly, this was not observed in the original AniA-thrombin-His protein. Clearly, the potential stability of this C-terminal region warrants further investigation.

3.3 AniA-3c-His and His-3c-AniA

Since the two tagged protein constructs described above appear susceptible to two different proteases, we hypothesised that the C-terminal truncation issue could be remedied by appropriate selection of a protease cleavage site. As the final approach in this project, we designed the AniA protein to be expressed with a hexa-His tag that can be cleaved by the 3c protease. This protease has a longer target recognition sequence (Table 3.1), which should further suppress non-specific cleavage of the target protein. To maximise the likelihood for success, we introduced the tag at either the N- or the C-terminus. These where successfully overexpressed in Codon+, Rosetta2 and Rosetta pLySs strains of *E. coli* (Figure 3.5a)

Before proceeding with purification and cleavage of hexa-His tag, we decided to examine whether the 3c protease would non-specifically target the susceptible C-terminal region in AniA. To test this,

purified AniA protein from the thrombin purification approach was used as the test substrate. A T7 protein (kind gift from Dr Liz Morris, Department of Biosciences) was used as a positive control. The results can be seen in figure 3.5b. Before addition of the 3c protease, the AniA sample produced two bands, corresponding to the full-length (higher molecular weight band) and truncated (lower molecular weight band) AniA proteins. After addition of the 3c protease, the higher molecular weight band disappeared and only the lower molecular weight band remained, suggesting that 3c protease also cleaved full-length AniA at the C-terminus non-specifically. Therefore, purification of the 3c-AniA constructs were not pursued further.

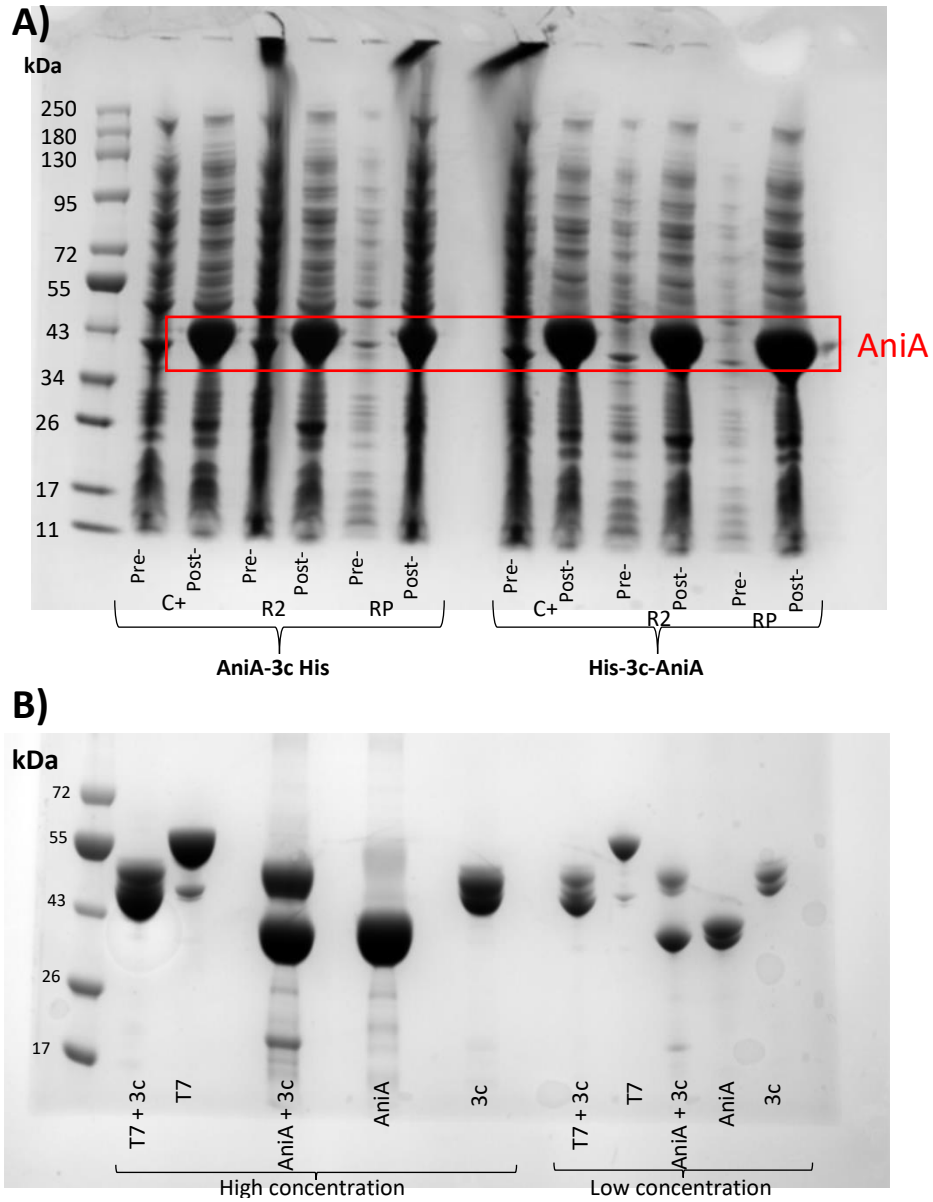

Figure 3.5: **A)** Protein gel showing overexpression His-3c-AniA and AniA-3c-His in Codon+ (C+), Rosetta2 (R2) and Rosetta pLySs (RP) pre and post induction with IPTG. **B)** Protein gel showing the results of trial cleavage of apo-AniA with 3c protease.

Chapter 4: Investigating Cu loading into *apo*-AniA .

The active *holo*-AniA enzyme is known to be a functional homotrimer [54]. As discussed in Chapter 2, each protomer of AniA contains one T1Cu and one T2Cu binding sites. Notably, the T2Cu site is located at the interface between two neighbouring polypeptides with the Cu ion binding His-139 and His-174 from one polypeptide, and His-329 from the neighbouring polypeptide. However, recent research in the Djoko Lab indicated that *apo*-AniA is a monomer in solution, as evidenced by its elution profile on an analytical size exclusion column [59]. This result suggests that trimerisation and metalation of AniA are linked.

In *N. gonorrhoeae*, AniA most likely receives Cu from the periplasmic Cu-binding metallochaperone AccA [61] . However, the molecular details for Cu transfer from AccA to AniA are not yet known. Therefore, for this project, we chose to examine the link between metalation and trimerisation of AniA using aqueous copper. Although this simplified approach does not fully represent the physiological situation, it does have physiological relevance. AniA activity in an *N. gonorrhoeae accA*$^{-}$ knockout mutant strain can be recovered by supplementing the growth medium with Cu salts [59,61]. Thus, AniA can receive Cu from the periplasmic buffered Cu pool in the absence of AccA. The results of this study and technical understanding developed in this study would also help inform future research into Cu transfer from AccA.

4.1 End point UV-vis spectroscopy experiments.

4.1.1 T1Cu site loads before the T2Cu site.

One immediate question posed by the presence of two different Cu binding sites is whether or not there is an order to the Cu insertion process. Does Cu insert into one of the sites first or does Cu

insert into both sites at simultaneously? To investigate this, we performed a series of Cu titrations in which increasing molar equivalents of Cu were added to purified recombinant *apo*-AniA. UV-vis spectrophotometry was used to track Cu insertion into the T1Cu site, which when metalated develops characteristic solution absorbances at 460 nm and 600 nm [64] (Figure 4.1).

As shown in Figure 1b and c, adding up to one molar equivalent of Cu led to a linear increase in the solution absorbance intensities at both 460 nm and 600 nm. Additional Cu did not increase these intensities further. This result indicates that Cu preferentially inserts into the T1Cu site over the T2Cu site. It is consistent with previous research by Dr S Firth, who showed that the T1Cu site is also preferentially loaded when Cu is transferred from *holo*-AccA [59].

Preferential insertion into the T1Cu site could be either a kinetic or thermodynamic effect. It should be noted that absorbance readings were recorded after at least 2 hours. Therefore, this result is likely a thermodynamic effect and that the T1Cu site has a tighter binding affinity than the T2Cu site.

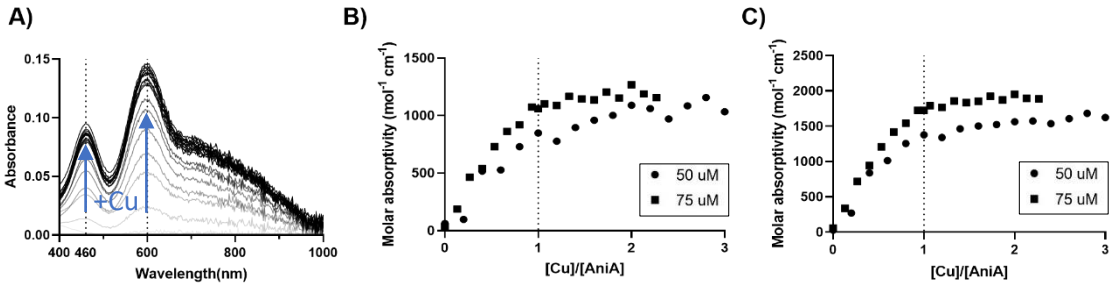

Figure 4.1 Cu titration into AniA: **A)** Whole spectrum of AniA showing increase in absorbance with addition of Cu. **B)** Increase in absorbance at 460 nm as Cu is titrated into *apo*-AniA at either 50 µM or 75 µM **C)** Increase in absorbance at 600 nm as Cu is titrated into *apo*-AniA at either 50 µM or 75 µM

.

4.1.2 T1Cu site competes with NTA for Cu(II).

To estimate the Cu-binding affinity of the T1Cu site, we competed *apo*-AniA with a series of ligands with known affinities for Cu(II), ranging from $K_D = 2 \times 10^{-19}$ to $K_D = 7.9 \times 10^{-11}$ M.

Table 4.1: Affinities of Competitor ligands.

Competitor Ligand	Affinity (K_D)
EDTA (Ethylenediaminetetraacetic acid)	2×10^{-19} M [65]
EGTA (Ethylene-bis(oxyethylenenitrilo)tetraacetic acid)	2.5×10^{-18} M [65]
NTA (Nitrilotriacetic acid	1.0×10^{-13} M [66]
DP-3 (Dansyl peptide 3)	6.3×10^{-13} M [67]
DP-2 (Dansyl peptide 2)	7.9×10^{-11} M [67]
DP-1 (Dansyl peptide 1)	1.0×10^{-8} M [67]

The results (Figure 4.2) shows that when higher-affinity competitors such as EDTA and EGTA were present, adding 2 molar equivalents of Cu ions did not produce an increase in the absorbance intensity of AniA at 600 nm. This result suggests that EDTA and EGTA prevent Cu from binding to the T1Cu site. Therefore, the affinity of this T1Cu site is likely lower than those of EDTA or EGTA. In contrast, in the presence of the lower-affinity competitors DP-2 and DP-3, adding Cu increased the absorbance intensity of AniA at 600 nm to the same extent as adding Cu in the absence of a competitor ligand. This result suggests that the T1Cu site is loaded with Cu and that AniA has a higher affinity for Cu(II) than DP-2 and DP-3. Finally, in the presence of NTA, AniA developed some absorbance at 600 nm, albeit less intense when compared with the absence of a competitor (Figure 4.2). This suggests that NTA and AniA competed with each other for Cu(II), and that AniA must therefore have a similar Cu(II)-binding affinity to NTA.

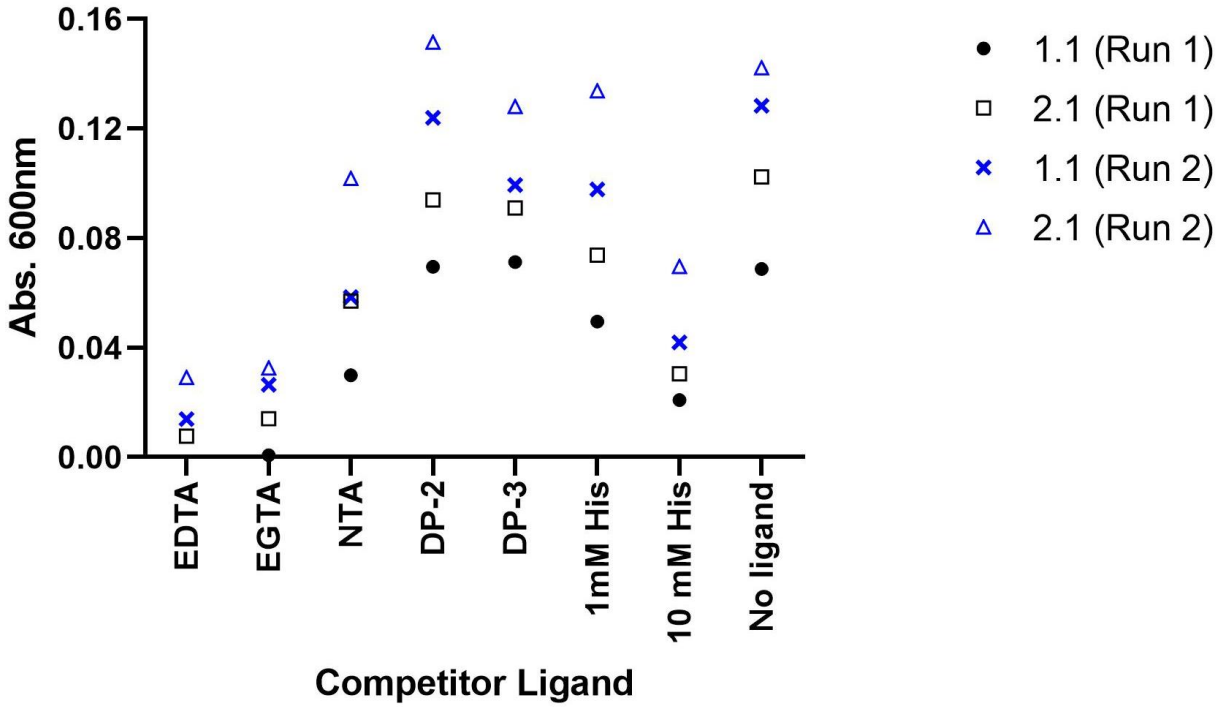

Figure 4.2: Absorbance at 600nm of AniA when mixed with 1 and 2 equivalents of Cu in the presence of different competitor ligands. Results from the first experiment are shown in black and whilst results from the duplicate experiment are shown in blue.

This work can be built upon to better estimate the Cu(II)-binding affinity for the T1Cu site. This would involve titrating either Cu, AniA, or NTA into a solution containing the other 2 reagents. The changes in solution absorbances at 460 nm and 600 nm throughout the titration can then be plotted and curve-fitted in DynaFit (Biokin Ltd) to calculate an Cu(II)-binding affinity for AniA [59,68]. However, this work should be undertaken using full-length AniA, in case the truncated domain influences Cu loading.

One weakness of our approach is that it assumes that the T2Cu site does not also compete with NTA. Given that the T1Cu site is preferentially loaded over the T2Cu site (as shown in Figure 4.1), this is probably an appropriate assumption. To remove the risk of T2Cu site competition, an AniA mutant lacking the T2Cu ligands could be used. However, this approach assumes that mutations to the T2Cu

site does not influence Cu loading to the T1Cu site. Given the proximity of the two sites, this is likely not an appropriate assumption, but nevertheless should be tested.

4.2 Kinetic UV-vis spectroscopy experiments.

While conducting the titration experiments described above, we observed that the characteristic blue colour of the T1Cu centre developed slowly. Therefore, we tracked the changes in solution absorbance intensities at 460 nm and 600 nm over time following the addition of Cu to a solution of purified *apo*-AniA. In this experiment, a reading was taken every 30 seconds post-addition of 1 molar equivalent of Cu to *apo*-AniA. As shown in Figure 4.3, the two absorbance intensities did not increase at the same rate. This effect was most apparent after plotting the ratio in the intensities at 460 nm:600 nm. This ratio started high at >2 but over time decreased to around 0.7, which was consistent with the value expected from the literature [64].

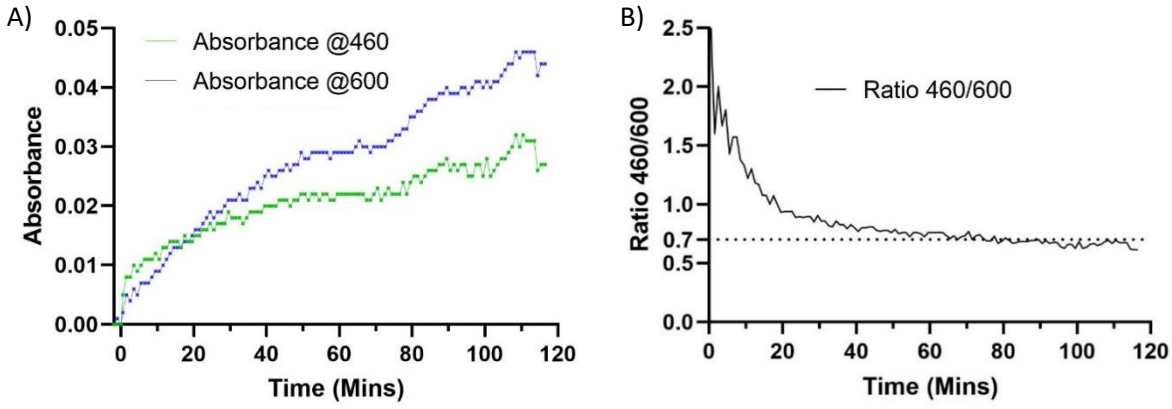

Figure 4.3: Kinetic UV-vis spectra of metalation of AniA with 1 equivalent of Cu, showing A) the formation of characteristic absorbances at 460 and 600 nm and B) how the ratio of 400nm/600nm absorbances alters during the reaction.

To determine whether the results are influenced by Cu concentrations, we repeated the experiment using varying molar equivalents of added Cu. The results in Figure 4.4 show that the rate of increase in 460 nm is independent of Cu concentration. In contrast, the rate of 600 nm formation and the rate at which the ratio returns to the reported literature value were increased with higher Cu concentrations.

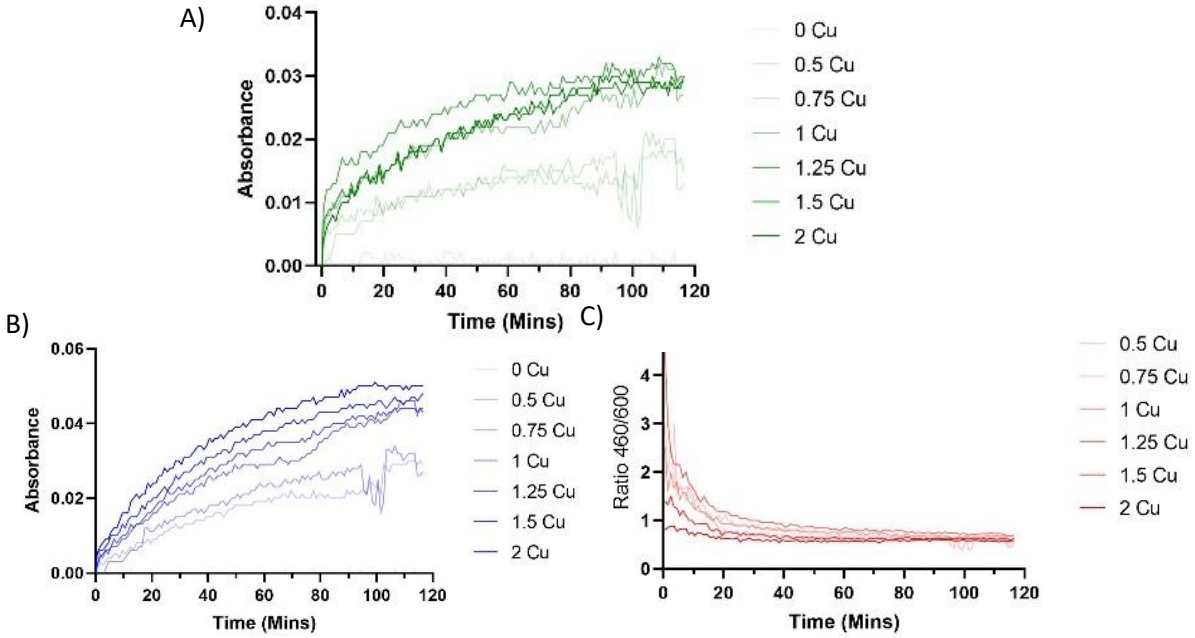

Figure 4.4: Kinetic UV-vis spectra showing how the formation of A) absorbance at 460nm and B)600nm, as well as C) the ratio of 460nm/600nm, changes along with different Cu concentrations.

The first thing to note from these results is that the absorbances at 460 nm and 600 nm increased immediately and slowed down with time. This result is consistent with a model in which the T1Cu site is the preferred kinetic product in the reaction between AniA and aqueous Cu, and that Cu is not inserted via the T2Cu site. If the T2Cu site had loaded first we would expect to see more sigmoidal curve. The initial rate of T1Cu centre loading would be zero as no T2Cu centres would have formed. As T2Cu centres form the rate of T1Cu centre increase accordingly. Finally, T1Cu centre formation will decrease to zero as the concentration of either *apo*-AniA and aqueous Cu in solution decrease to zero.

The initial higher ratio of the absorbance intensities at 460 nm:600 nm would classify the T1Cu centre as a “green” Cu centre. This contrasts with the lower final ratio, which would classify the T1Cu centre as a “blue” Cu centre. The different absorbance ratios are a result of different geometries of ligand binding around the T1Cu centre [69] (Figure 5). The 2 different absorbances result from different orbitals within the S(Cys)-Cu bond. The 460 nm absorbance is the result of excitation of electrons found in the σ-bond, whilst the 600 nm absorbance results from the excitation of electrons found in the π-bond[70]. The ratios recorded from “green” T1Cu centres are therefore a result of a longer and weaker S(Cys)-Cu bond with greater σ character[71]. In contrast, the ratios recorded from “blue” T1 centres are the result of shorter and stronger S(Cys)-Cu bond with greater π character[70]. These different bond lengths result in two energy geometries which occupy two energy minima.

In “green” T1Cu centres, the S(Cys)-Cu bond and the S(Met)-Cu bond are of similar lengths, creating an orbital degeneracy. Cu centres with degenerate orbitals take advantage of the Jahn-Teller effect[20], where elongation of bonds along the *z*-axis stabilises electron-containing orbitals. To maximise this effect “green” T1Cu centres form a flatter, more square-planar coordination geometry, which maximises differences z-displacement between bonds. They are however prevented from forming a true square planar geometry by the energetic penalty associated with increased steric crowding.

The shorter short S(Cys)-Cu bond of the “blue” T1Cu centre is also accompanied by a longer S(Met)-Cu bond. This breaks the orbital degeneracy of the T1Cu centre preventing the Jahn Teller effect. Flatter geometries therefore provide no energetic benefit and consequently “blue” T1Cu centres form less sterically confined tetrahedral conformation.

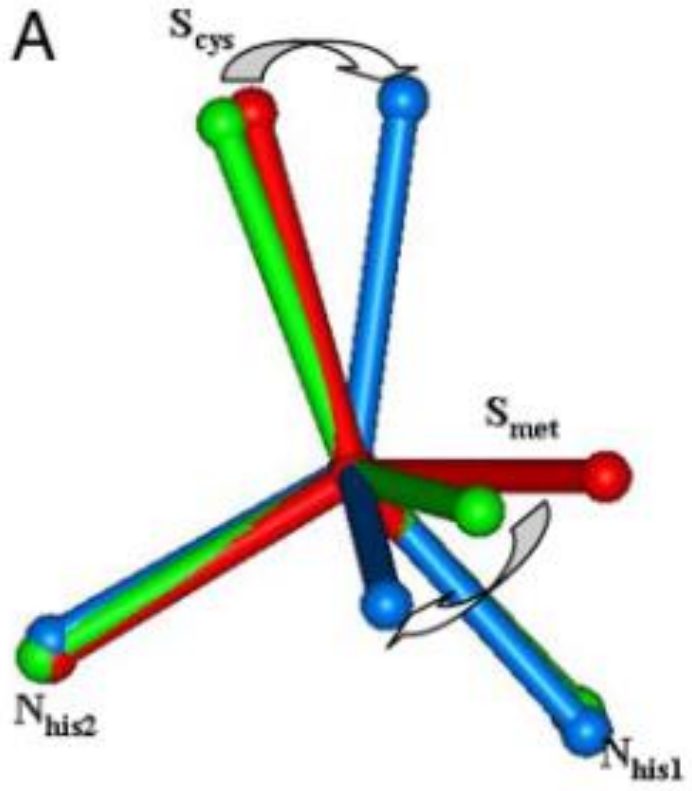

Fig. 4.5: Taken from Thermodynamic equilibrium between blue and green copper sites and the role of the protein in controlling function this shows the different geometries of blue, green and red T1Cu centres[69].

Applying this information to the results in Figure 4.3, we can hypothesise that formation of the T1Cu centre in AniA takes place in two stages: initial Cu binding to the site forms a "green" T1Cu centre as a reactive intermediate species. This product subsequently undergoes intramolecular transition to form the active "blue" T1Cu centre product. This gives the overall reaction pathway show in Eq. 4.1:

Eq. 4.1 $$apo.AniA + Cu \rightarrow [Cu(AniA)]_{Green} \leftrightarrow [Cu(AniA)]_{Blue}$$

The "green" and "blue" T1Cu centres are conformers of each other. In the absence of additional structural constraints, there should be a low energy barrier for the transition between them, as the

geometries are so similar. As such, at any given time in the reaction, the T1Cu centre will have the most stable geometry within the structure of the polypeptide that it is coordinated to. The transition from “green” to “blue” T1Cu centre must therefore reflect a change in structure of the polypeptide. This raises the question: what structural change in the polypeptide is responsible for the observed change in T1Cu centre geometry?

The relative stabilities of the “green” and “blue” T1Cu centres likely result from 3 competing energetic effects:

1) Bond energies: “Green” and “blue” T1Cu centres have different Cys-Cu and Met-Cu bond lengths. Each of these bonds will have a favoured bond length for optimal ligand-metal orbital overlap. Deviations from this favoured length will carry an energetic penalty. Changes in the electronic structure of Met or Cys will change the favoured bond length, altering the relative bond energy of the “green” and “blue” T1Cu centres. This could occur due to hydrogen bonding to the sulfur, which would affect their electron-donating ability [72,73] .

2) The Jahn-Teller effect: as discussed above, “green” T1Cu centres take advantage of the Jahn-Teller effect whilst “blue” T1Cu centres cannot. The size of the Jahn-Teller effect is independent of the polypeptide structure and will always favour “green” sites.

3) Steric effects: “Green” and “blue” T1Cu centres position their ligands differently in 3D space, with “green” centres being in a flatter and more crowded square-planar like geometry whilst “blue” centres have a less crowded tetrahedral geometry. When a polypeptide folds or undergoes a conformational change, the position of its amino acid residues shift as they move towards more stable tertiary structures. Each of these different conformations will place different steric strain on “green” and “blue” T1Cu centres.

We hypothesis a change in the size of one of these energetic effects is responsible for the shift in geometry.

It is true that crystal structures of the active *holo*- AniA trimer show that Cys-175 is hydrogen bonded to neighbouring Val-177 and Asn-135 (Figure 4.6). Based on their positions and orientations, we hypothesise that these hydrogen bonds are also present in the "green" AniA intermediate. Therefore, changes in bond energy unlikely to be the cause of the geometric shift. The thermodynamics of hydrogen bond formation is defined by the relative sizes of the enthalpic release of energy and the associated reduction of entropic freedom (Eq. 4.2). Asn-135 directly neighbours His-134 while Val-177 is only one amino acids away from Cys-175. Therefore, once the T1Cu centre forms, these amino acids likely already have low entropic freedom and hydrogen bond formation would be thermodynamically favourable.

Moving one step further, we hypothesise that these hydrogen bonds are responsible for the formation of the vacant T1Cu site in *apo*-AniA, ready to receive a Cu ion. Another issue with the "bond formation" mechanism is the timeframe of the process. Intramolecular bond formation is usually a rapid process, far faster that the "green" to "blue transition recorded in our study, which took many minutes to complete.

Eq4.2. $$\Delta G = \Delta H - T\Delta S$$

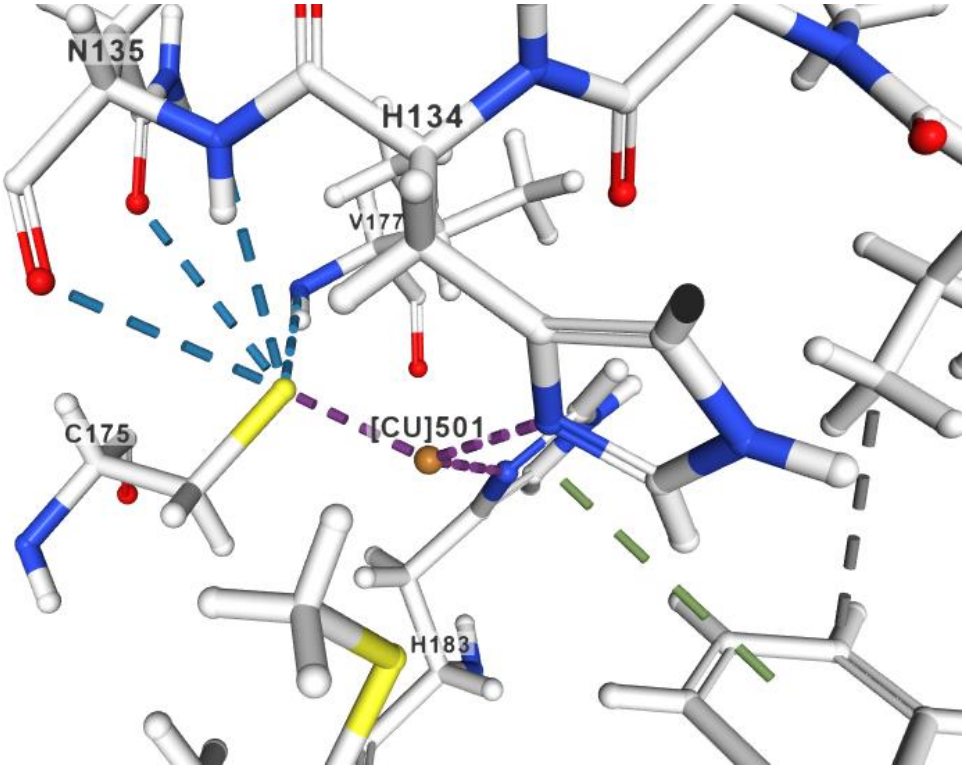

Figure 4.6: T1Cu bind site showing hydrogen bonding (----) of Cys175 to Asn135, His 134 and Val177 [54,74].

Instead, we propose a change in steric effects is more likely to be the cause of the geometric transition. Following Cu insertion into the T1Cu site, AniA must undergo further conformational change from the more flexible structure, which we propose exists in the monomeric *apo*-form, to the more rigid structure recorded in the active, trimeric *holo*-form. As AniA readjusts its conformation, the reduction in flexibility will increase the effective steric bulk of each of the coordinating amino acid ligands around the T1Cu centre, leading them to favour the less crowded "blue" geometry. The protein folding process is also a slower process, which matches better with the rate of "green" to "blue" transition recorded in this experiment.

The reduction in flexibility responsible for the geometric transition does not have to come from protein folding alone, instead it may be amplified by protein trimerisation. The equilibrium between

the monomeric and trimeric forms of AniA will be determined by relative sizes of exothermic bond formation at the trimer interfaces (-ΔH) and loss entropic freedom (-ΔS) caused by a trimerization event. Using Eq. 4.2 we can see that for trimerization to be favoured, the exothermic nature of bond formation must overcome the loss of entropic freedom. The flexible *apo*-AniA will have high entropic freedom, meaning the -ΔS component of trimerization will be large but Cu binding into the T1Cu site likely reduces some entropic freedom making -ΔS will be smaller. Cu insertion into the T1Cu site may therefore make trimerisation more thermodynamically favourable. Trimerisation in turn decreases flexibility increasing the effective steric bulk around the T1Cu centre which favours the "blue" geometry.

There was a positive correlation between the concentration of copper, the rate of formation of absorbance at 600 nm, and the rate of ratio shift (Figure 4.4). This result suggests that the rate of the overall reaction from *apo*-AniA to *holo*-"blue"-AniA is Cu-dependent. However the picture becomes more complex because, our preliminary data also suggests that the formation of absorbance at 460 nm is independent of Cu.

It is impossible to empirically calculate the proportion of "green" and "blue" T1Cu centres in solution at any given time because the extinction coefficient of the "green" T1Cu site is unknown. However, we can consider from first principles how this proportion may fluctuate with changes in Cu concentration. If we plot the total solution absorbance at 460 nm *vs* time in low Cu conditions, we can plot a second theoretical line to represent the absorbance of the "blue" T1Cu centre (Figure 4.7a). The area under this second line represents the amount of "blue" T1Cu centre whilst the area between two curves represents the amount of "green" T1Cu centre.

Next, we can hypothesise what the graph would look like for high Cu conditions (Figure 4.7B). Absorbance at 460 nm is independent of Cu concentrations therefore total absorbance is

unchanged. Since the rate of “blue” T1Cu centre formation is proportional to Cu, the second line should be plotted higher. The area representing the “green” T1Cu centre is thus smaller. Therefore, we hypothesise that the concentration of the “green” T1Cu centre formed during Cu insertion is inversely proportional to Cu concentrations.

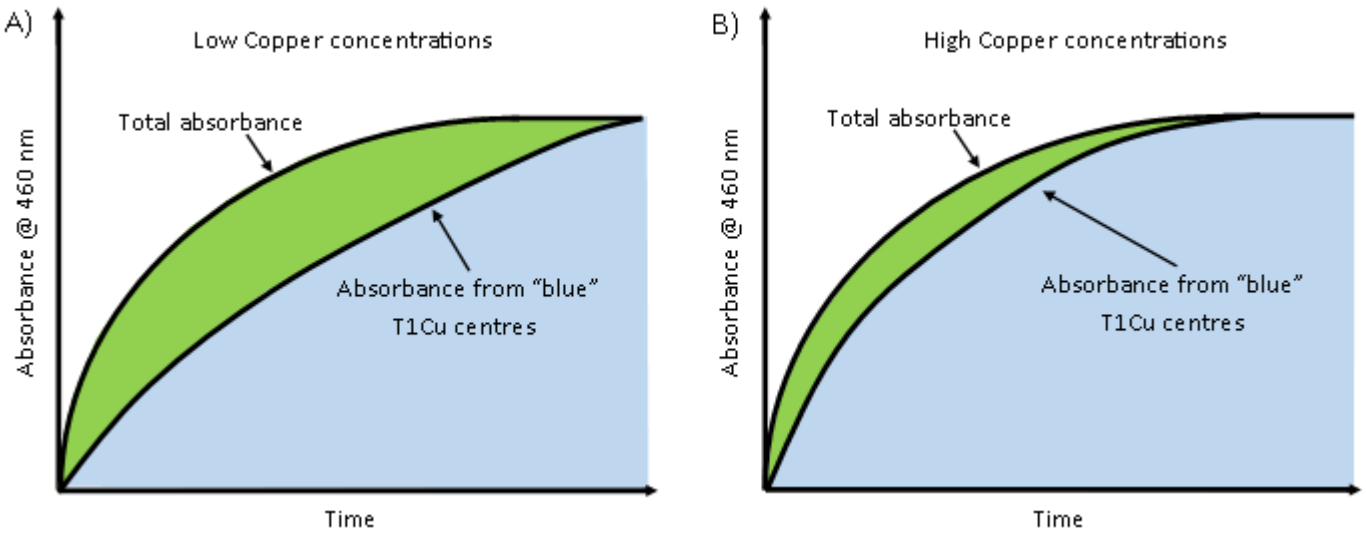

Figure 4.7: Theoretical proportions of 460 nm absorbance coming from “green” and “blue” sites in **A)** low and **B)** high concentrations of copper.

We can use rate equations to consider the kinetic factors responsible for this effect:

Eq 4.3: [T1Cu(green)] ≈ (rate of Cu binding) – (rate of intramolecular transition)

This suggests that the increased copper increases rate of intramolecular transition more than the rate of Cu binding. We would predict that Cu binding should be highly Cu dependent whilst the rate of intramolecular transition should be independent of copper. As our results show the inverse is true this creates two questions:

1) Why might Cu binding be less Cu dependent that expected?
2) Why is the rate of intramolecular transition Cu dependent?

We hypothesis that the reason Cu binding be less Cu dependent that expected is because a pre-folding stage may instead be rate limiting. The flexibility of *apo*-AniA described previously in chapter 3 means that *apo*-AniA can access a wide range of folded state. It is possible that only a small subset of these folded states can bind copper. For those proteins in states that cannot bind Cu a folding reaction is therefore necessary before insertion can occur. If the number of folded states that can bind Cu is low and the interchange between folded states is slower than the rate of Cu binding folding can become rate limiting reducing the impact of Cu concentrations on rate. One potential theory is that the folded state which can bind Cu is in fact the trimerized state. However crystal structures of trimerized Holo-AniA show the T1Cu site is buried within the structure making it less not more accessible. It is therefore unlikely that trimerization is initial rate limiting step.

We hypothesise that the rate of intramolecular transition is Cu dependent because its rate is increased by Cu binding in the T2Cu site. The intramolecular transition still occurs at concentrations of Cu bellow one equivalent, where according to our previous experiments (Figure 4.1) no Cu is bound to the T2Cu site. We therefore cannot say the transition is dependent on Cu binding in the T2Cu site however we suggest it makes it more thermodynamically favourable. This may occur because the T2Cu site is a rigid structure which holds its coordinated amino acid ligands in a specific geometry. Given its proximity to the T1Cu centre the formation of the T2Cu centre should therefore increase the effective steric bulk around the T1Cu centre which in turn favours the less crowded "blue" T1Cu centre.

T2Cu centre formation should also increase the rate of trimerisation. The rigidity it creates would reduce the -ΔS of trimerisation but T2Cu centre formation should increase the -ΔH of trimerisation.

The T2Cu site has ligands from both two different monomers in trimeric *holo*-AniA and the partially formed T2Cu centre found in monomeric AniA will be unstable. Formation of the full T2Cu centre which occurs during trimerisation would therefore cause a large exothermic release of energy. As discussed above increasing the favourability of trimerization in turn reduces flexibility, increases effective steric bulk and favouring the formation of a "blue" T1Cu centre.

Putting the above hypothesis together we can create a model mechanism for the insertion of aqueous Cu into AniA which is shown in Figure 4.8.

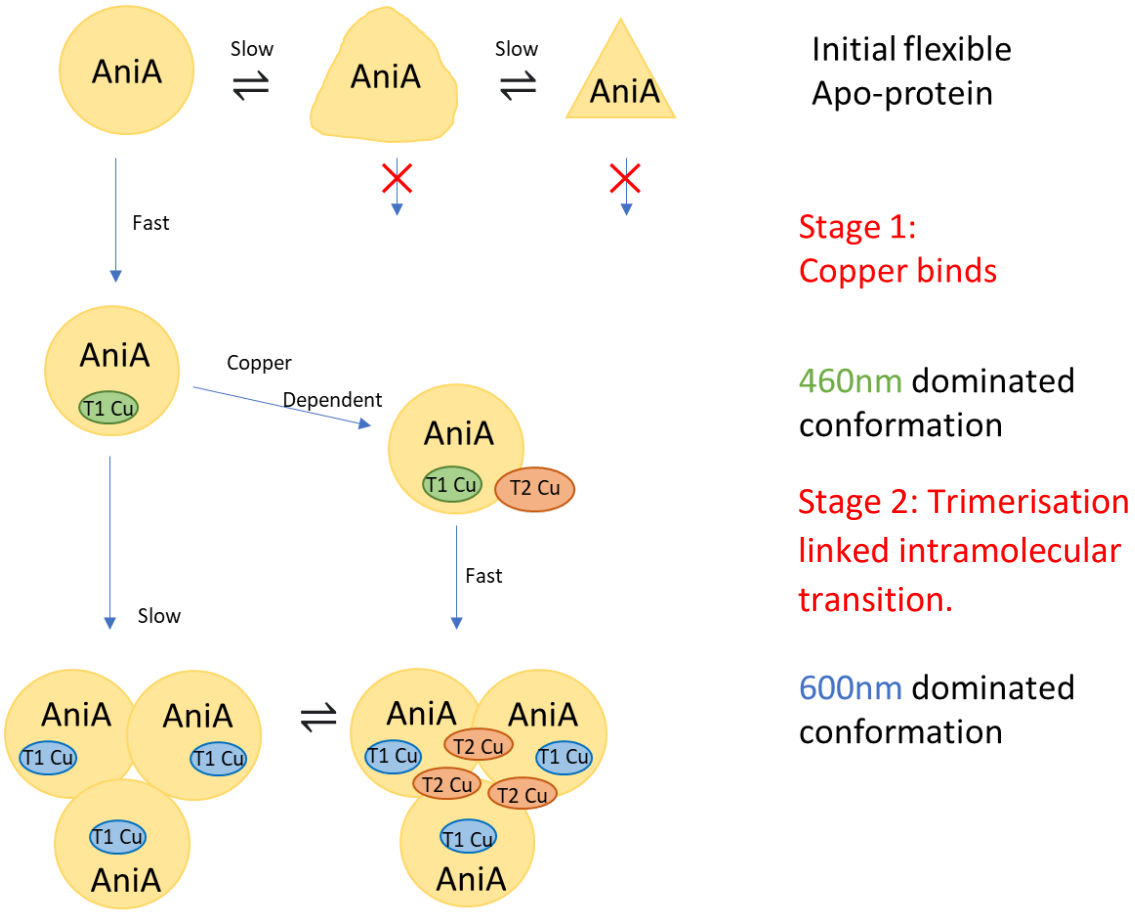

Figure 4.8: Model of Cu insertion into *apo*-AniA showing initial insertion into the T1Cu site of the flexible *apo*-AniA. This is followed by a intramolecular transition which is amplified by trimerization. This change can however be accelerated by insertion of Cu into the T2Cu site.

Implications and weakness of this model.

It is therefore worth considering how it might inform our understanding of metalation from AccA. A key feature of this model is that it suggests that Apo-AniA is a highly flexible monomeric species and that folding into the correct monomer is rate limiting in initial Cu metalation. It is therefore interesting to consider how AccA may act as a folding chaperone with its binding stabilizing the correct conformation of AniA. This chaperone effect of AccA could also be important *In vivo* as highly flexible proteins are very susceptible to protein-aggregation. AccA could therefore play a key role in preventing protein aggregation especially in Cu limited environments.

When considering this model, it is also important to consider how these results recorded *in vitro* may differ from the function of AniA metalation *in vivo*. Alongside the absence of AccA in these experiments AniA has been truncated removing its N-terminal membrane binding domain however little is known about how this may affect the function of the protein [75]. Another key difference between *in vitro* and *in vivo* systems is the concentration of protein present. *In vitro* systems are highly diluted and therefore lack the molecular crowding effect as well as protein-protein interactions which can affect the stability of different folded states. This crowding effect tends to favour trimerization events and therefore it is quite possible that though the apo form of AniA is monomeric *in vitro* it is trimeric in *in vivo* [76].

It is also important to note that this model is only based of a single source of experimental evidence which reports only on formation of the T1Cu site. The timing of trimerization and folding events as well as the effect of T2 Cu binding are therefore only speculative. As such further kinetic studies need to be carried out.

4.3 Fluorescence spectroscopy experiments.

A major challenge in studying Cu insertion into AniA is the spectroscopically silent nature of the T2Cu centre. T2Cu centres do not have UV-vis absorbance features that can be conveniently measured. Whilst other techniques such as EPR do record features associated with T2Cu centres [77] they require a prohibitively large quantity of protein. In addition, Durham University lacks the required equipment.

The aromatic amino acids Tyr and Trp can imbue proteins with fluorescence emission around 330 nm if excited around 290 nm. The literature shows that the presence of Cu nearby can cause a 50-fold reduction in fluorescence [78,79] . X-ray crystal structures of *holo*-AniA show that 3 Tyr residues lie in close proximity to each T2Cu centre as well as a Trp residue in close proximity to each T1Cu centre (Figure 4.9). Therefore, we hypothesised that insertion of Cu into the T2Cu site will quench AniA fluorescence.

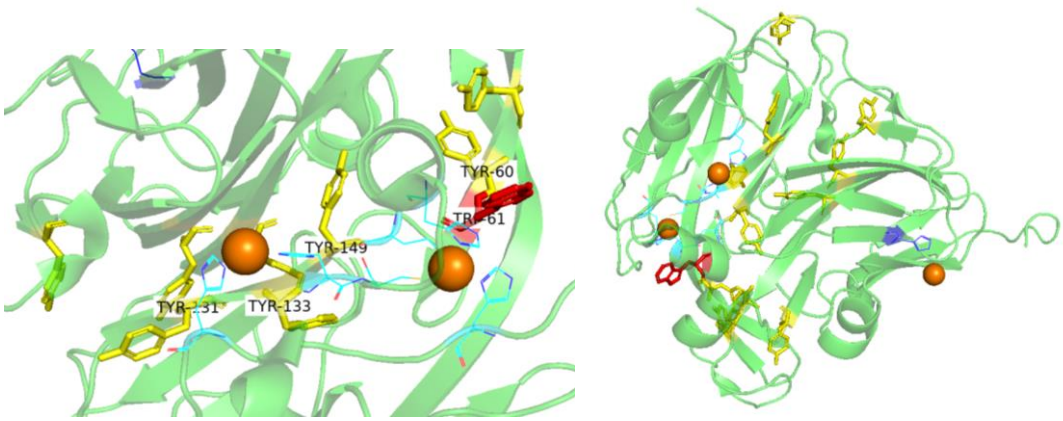

Figure 4.9: Crystal structure of AniA highlighting the position of fluorescent amino acids. Tyrosine residues are shown in yellow and the Tryptophan residue is shown in red. Copper binding amino acids are shown in stick form**. A)** Shows a close-up view of fluorophores likely to be quenched by the

T1Cu and T2 Cu centres. **B)** Shows an entire monomer showing the position of all fluorophores relative to the T1Cu and T2 Cu centres [54,60].

The initial experiments compared the fluorescence of purified *holo*- and *apo*-forms of AniA. These experiments also helped to refine the experimental procedure including the excitation point and the emission wavelength. The results (Figure 4.10) did show a clear reduction in the fluorescence emission intensity of the *holo*-AniA when compared with *apo*-AniA. The fluorescence emission wavelength was also blue-shifted, namely from 340 nm for *apo*-AniA to 305 nm in *holo*-AniA. This indicates *apo*-AniA fluorescence is dominated by Trp, which emits at higher wavelengths of 330-450 nm, depending on solvent accessibility [80] . In *holo*-AniA, Tyr is the predominant fluorophore, as Tyr is known to emit at a lower wavelength around 310 nm [81,82] .

Though this experiment showed the overall change in fluorescence intensity, it did not indicate weather quenching occurred during T1Cu insertion, T2Cu insertion, or both. To determine this, Cu was titrated into an *apo*-AniA solution and the fluorescence emission after each addition of Cu was recorded. The results (Figure 4.10A and 4.10B) showed that both quenching and blue-shifting occurred in response to the first molar equivalent of added Cu. As shown previously in Figure 4.1, the first equivalent of Cu enters the T1Cu site. This is consistent with our hypothesis that fluorescence for *apo*-AniA largely comes from Trp, which is located near the T1Cu site. Adding more Cu into the protein, which would load the T2Cu site, did not lead to any further change in the fluorescence emission (Figure 4.10C). Therefore, protein fluorescence cannot be used as a method to track loading of Cu into the T2Cu site of AniA.

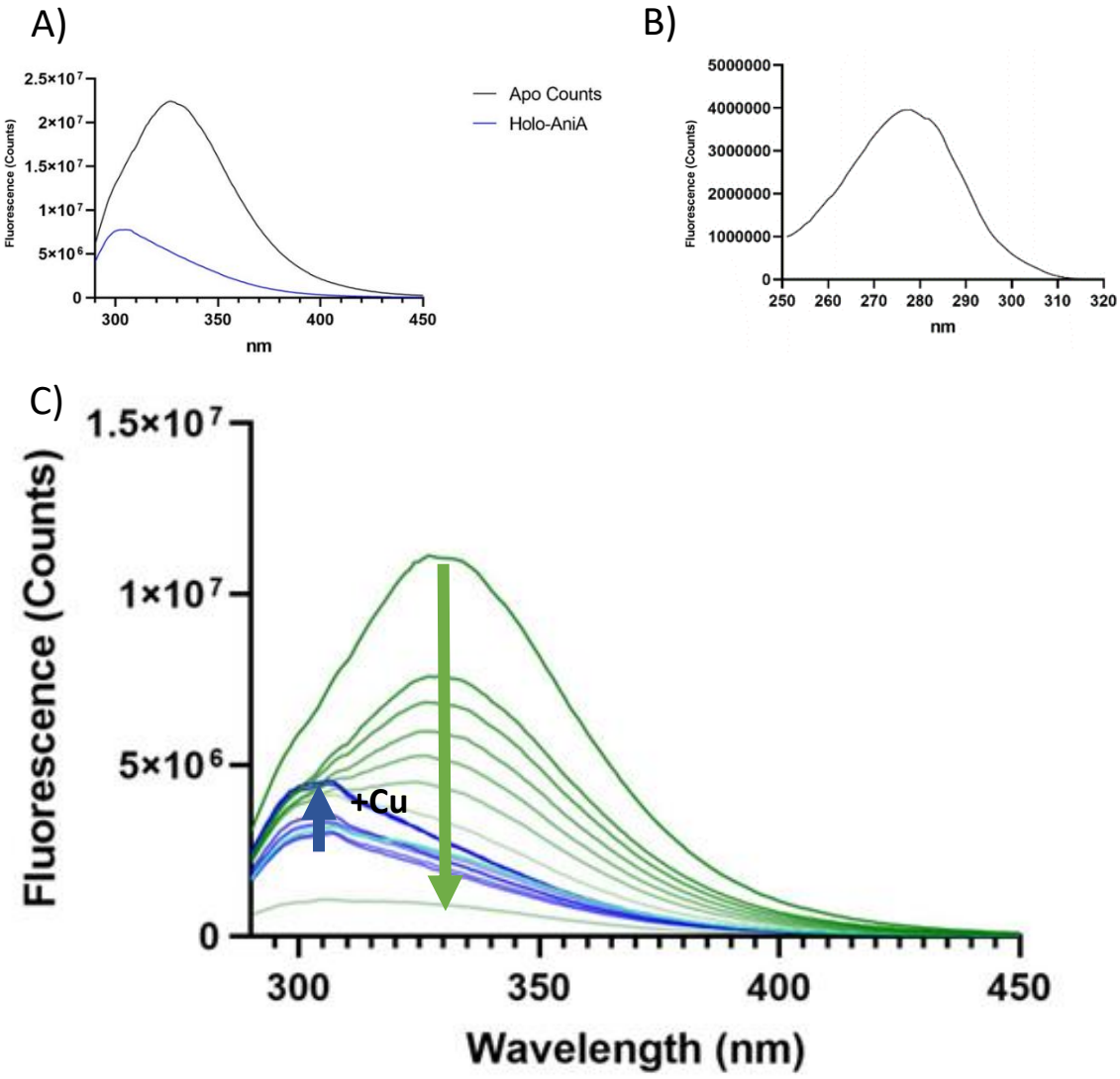

Figure 4.10: Fluorescence data for AniA. **A)** Emission spectra of *holo*-AniA and *apo*-AniA**.** **B)** Excitation spectrum of *apo*-AniA**. C)** Emissions spectra from Cu titration into AniA showing the addition of the first equivalent of Cu in green and the second equivalenting blue

4.4 Potential future experiments for measuring T2 Cu loading, protein folding, and trimerisation.

To test the various Cu insertion hypotheses outlined above, methods must be developed to track loading of Cu into the T2Cu site and protein trimerisation, alongside loading of Cu into the T1Cu site.

Using non-competitive metal probes.

One methodology for measuring occupancy of T2Cu site would be to use a non-competitive colorimetric or fluorometric metal probes to measure the concentration of Cu ions that are not bound to AniA. By assuming that all Cu in solution is bound either by the T1Cu site, T2Cu site, or fluorescent probe, the equation bellow can be used to calculate the occupancy of the T2Cu site:

Eq.4.4: $$Cu^{T2} = Cu^{total} - Cu^{T1} - Cu^{Probe}$$

Potential candidates would be the DP-2 or DP-1 probes used earlier. These probes are fluorescent and quenched upon binding Cu. The experiments in figure 4.2 show that DP-2 does not compete with the T1Cu site. We hypothesise that DP-2 compete with the lower affinity T2 Cu site or alternatively the weaker DP-1 probe (Table 4.1) could be used [67]. The competition curves can be used to calculate the affinities of the T2Cu site using DynaFit (Biokin LTD). Since we can simultaneously track the T1Cu centre, this methodology also has the advantage of being able capture potential competition or cooperative interactions between the 2 Cu-binding sites.

Using fluorometry.

The difficulty with our fluorometry experiments with AniA so far is not with collecting the data but instead with interpreting the results. Derivative fluorometry could be used to analyse our Cu titration curves. Higher dimension derivatives separate out the contributions of different fluorophores within a protein, allowing more detailed information to be gleaned [81,83] .However, these higher order derivatives are more susceptible to noise, and as such more repeats and a more accurate experimental method would be necessary. Mutants, such as a Trp-101 knockout mutant, could also be used to simplify the spectrum, assisting the assignment of peaks. Once derivative

fluorometry has been used to properly understand the impact of different fluorophores, Kinetic or time-course studies using fluorescence also show some promise.

Using of Mass Photometry.

Dr S Firth in the Djoko Lab previously used mass photometry to distinguish between the monomeric and trimeric forms of AniA [59] . This technique uses a microscope to track the relative populations of protein sizes in solution [84] . However, it is currently not clear whether these distribution results are quantitative [85] .Nevertheless, mass photometry holds the potential to capturing other oligomeric intermediates of AniA, or complex formation between with the metallochaperone AccA. It can also be applied to study lipid-bound proteins, allowing the effect of the lipid-binding portion of AniA on protein metalation and trimerisation to be examined [86] .

Using 2D-NMR

2D-NMR detects changes in the environment surrounding ^{15}N atoms and relative positions of ^{1}H and ^{15}N atoms [87] . Using ^{15}N-labelled AniA protein, this technique would theoretically allow us to track insertion of Cu into T1Cu and T2Cu sites, changes in protein folding [88], and trimerization [89] . During folding and trimerization events, ^{1}H and ^{15}N atoms will move relative to each other, causing peak shifts. Cu(II) ions are paramagnetic and therefore interacts strongly with both ^{1}H and ^{15}N atoms in its immediate proximity, causing line broadening. Since formation of the T1Cu centre (and presumably that of the T2Cu centre and trimerisation) is slow, occurring over more than an hour and thus much slower than spin relaxation rate, 2D-NMR can be used to track both end points and time dependence [90] .

2D-NMR data can also be used to determine the structure of *apo*-AniA in solution [91] , which is currently unknown. This information would provide the initial conformation or fold of an AniA protomer before insertion of Cu, which we hypothesise is different from that of the final metalated conformation. Furthermore, we hypothesised earlier that *apo*-AniA is flexible or that it carries a flexible domain that is susceptible to proteolytic cleavage. This flexible domain may prevent structural studies by X-ray crystallography but may be amenable to studies by 2D-NMR. This technique may also be used to study AniA when bound to a phospholipid membrane or even AniA *in vivo* [91,92].

Chapter 5 - Conclusion

One of the main findings from this project has been the potentially flexible nature of the *apo*-AniA monomer (or at least a C-terminal domain), which undergoes conformational rearrangement to become the rigid active-trimer during the metalation process. Evidence of this flexibility could be seen in the susceptibility of *apo*-AniA to non-specific cleavage by different proteases during and the transition from the "green" to "blue" T1Cu centre. A follow-up study using molecular dynamics simulation by a new student in the Djoko Lab supported this hypothesis. Given this we can consider how this result may affect wider literature on both AniA and other NirKs. One question is whether this flexible *apo*-form is ubiquitous across all NirKs or whether it is a unique feature of AniA. There is no literature that describes the nature of *apo*-NirK and its metalation process. Instead, NirK research has focused on the structure and function of their active *holo*-forms.

It is worth noting that *holo*-AniA does have structural features that make it an outlier amongst the NirKs. AniA displays about half the specific activity of other NirKs and its T1Cu site has an unusual ratio of 460:600 nm absorbances. Structurally, AniA has shortened loops when compared to other Nik's which typically lack the ability to bind to membranes [93]. In Nik's the loops are thought to assist trimerization, the shortening of AniA's loops therefore would decrease the probability of trimerisation potentially causing *apo*-AniA's flexible monomeric structure. If this is the case our results are likely atypical within Nik's

This however raises the question of why AniA has evolved these features, particularly given they are associated with a decrease in enzyme activity. What evolutionary advantage to these changes give *Neisseria gonorrhoea?*

One theory is that the increased flexibility of *apo*-AniA has evolved to make it more susceptible to controlled protein degradation. The ability to efficiently digest *apo*-AniA may be beneficial to *N. gonorrhoeae* under 3 conditions: copper limited, iron limited, or oxygen-rich environments.

Copper ions are used other proteins within *N. gonorrhoea* for example azurins which are required to deal with oxidative stress [94,95] . This means under certain conditions, such as low copper and high ROS, it may be necessary to reduce copper binding to *apo*-AniA to prioritise metalation of other proteins. Copper limited conditions may also be a common occurrence for AniA due to nutritional immunity where host organisms reduce the availability of key nutrients like copper to fight infections [96].

Another form of nutritional immunity host use is reducing the availability of iron by producing protein siderophores like lipocalin [97] . This could be problematic for *N. gonorrhoea* as the second stage in their denitrification pathway is carried out by iron dependent protein NorB [48] . Cells with functional AniA by non-functional NorB are known to die due to a build-up in toxic NO [61] . As such if NorB is non-functional due to a lack of iron *N. gonorrhoea* would require a mechanism to reduce AniA activity. The degradation of *apo*-AniA could be one target to achieve this.

References

1. Thomson, A. J. & Gray, H. B. Bio-inorganic chemistry. *Curr Opin Chem Biol* **2**, 155–158 (1998).

2. Waldron, K. J., Rutherford, J. C., Ford, D. & Robinson, N. J. Metalloproteins and metal sensing. *Nature* **460**, 823–830 (2009).

3. 'Riordan, J. The role of metals in enzyme activity. *Ann Clin Lab Sci* **7**, 119–129 (1977).

4. Andreini, C., Bertini, I., Cavallaro, G., Holliday, G. L. & Thornton, J. M. Metal ions in biological catalysis: From enzyme databases to general principles. *Journal of Biological Inorganic Chemistry* **13**, 1205–1218 (2008).

5. Yamashita, M. M., Wesson, L., Eisenman, G. & Eisenberg, D. Where metal ions bind in proteins. *Proc Natl Acad Sci U S A* **87**, 5648 (1990).

6. Imlay, J. A. The mismetallation of enzymes during oxidative stress. *J Biol Chem* **289**, 28121–28128 (2014).

7. Robinson, N. J. & Glasfeld, A. Metalation: nature's challenge in bioinorganic chemistry. *Journal of Biological Inorganic Chemistry* **25**, 543–545 (2020).

8. Irving, H. & Williams, R. J. P. Order of Stability of Metal Complexes. *Nature 1948 162:4123* **162**, 746–747 (1948).

9. Dokmanić, I., Šikić, M. & Tomić, S. Metals in proteins: correlation between the metal-ion type, coordination number and the amino-acid residues involved in the coordination. *Acta Crystallogr D Biol Crystallogr* **64**, 257–263 (2008).

10. Pearson, R. G. Hard and Soft Acids and Bases. *J Am Chem Soc* **85**, 3533–3539 (1963).

11. Choi, T. S. & Tezcan, F. A. Overcoming universal restrictions on metal selectivity by protein design. *Nature 2022 603:7901* **603**, 522–527 (2022).

12. Osman, D. *et al.* Bacterial sensors define intracellular free energies for correct enzyme metalation. *Nat Chem Biol* **15**, 241–249 (2019).

13. Rono, J. K., Sun, D. & Yang, Z. M. Metallochaperones: A critical regulator of metal homeostasis and beyond. *Gene* **822**, (2022).

14. Robinson, N. J. & Winge, D. R. Copper metallochaperones. *Annu Rev Biochem* **79**, 537–562 (2010).

15. O'halloran, T. V & Culotta, V. C. Metallochaperones, an Intracellular Shuttle Service for Metal Ions* The Requirement for Copper Metallochaperones. *Journal of Biological Chemistry* **275**, 25057–25060 (2000).

16. Rosenzweig, A. C. Metallochaperones: Bind and deliver. *Chem Biol* **9**, 673–677 (2002).

17. Huffman, D. L. & O'Halloran, T. V. Energetics of Copper Trafficking between the Atx1 Metallochaperone and the Intracellular Copper Transporter, Ccc2. *Journal of Biological Chemistry* **275**, 18611–18614 (2000).

18. Capdevila, D. A., Edmonds, K. A. & Giedroc, D. P. Metallochaperones and metalloregulation in bacteria. *Essays Biochem* **61**, 177–200 (2017).

19. Heaton, D., Nittis, T., Srinivasan, C. & Winge, D. R. Mutational Analysis of the Mitochondrial Copper Metallochaperone Cox17*. (2000) doi:10.1074/jbc.M006639200.

20. Jahn, H. A. & Teller, E. Stability of polyatomic molecules in degenerate electronic states -. *Proc R Soc Lond A Math Phys Sci* **161**, 220–235 (1937).

21. Olejarz, J., Iwasa, Y., Knoll, A. H. & Nowak, M. A. The Great Oxygenation Event as a consequence of ecological dynamics modulated by planetary change. *Nat Commun* **12**, (2021).

22. Boal, A. K. & Rosenzweig, A. C. Structural biology of copper trafficking. *Chem Rev* **109**, 4760–4779 (2009).

23. Müller, M. & Azzi, A. Cytochrome c oxidase metal centers: location and function. *J Bioenerg Biomembr* **23**, 291–302 (1991).

24. Macomber, L. & Imlay, J. A. The iron-sulfur clusters of dehydratases are primary intracellular targets of copper toxicity. *Proc Natl Acad Sci U S A* **106**, 8344–8349 (2009).

25. Timoshnikov, V. A., Kobzeva, T., Selyutina, O. Y., Polyakov, N. E. & Kontoghiorghes, G. J. Effective inhibition of copper-catalyzed production of hydroxyl radicals by deferiprone. *J Biol Inorg Chem* **24**, (2019).

26. Wong, H. S., Dighe, P. A., Mezera, V., Monternier, P. A. & Brand, M. D. Production of superoxide and hydrogen peroxide from specific mitochondrial sites under different bioenergetic conditions. *J Biol Chem* **292**, 16804–16809 (2017).

27. Stadtman, E. R. & Levine, R. L. Protein oxidation. *Ann N Y Acad Sci* **899**, 191–208 (2000).

28. Auten, R. L., Whorton, M. H. & Mason, S. N. *Blocking Neutrophil Influx Reduces DNA Damage in Hyperoxia-Exposed Newborn Rat Lung*. *Am. J. Respir. Cell Mol. Biol* vol. 26 www.atsjournals.org (2002).

29. Fruhwirth, G. O. & Hermetter, A. Mediation of apoptosis by oxidized phospholipids. *Subcell Biochem* **49**, 351–367 (2008).

30. Migocka, M. Copper-transporting ATPases: The evolutionarily conserved machineries for balancing copper in living systems. *IUBMB Life* **67**, 737–745 (2015).

31. Bhattacharjee, A., Chakraborty, K. & Shukla, A. Cellular copper homeostasis: current concepts on its interplay with glutathione homeostasis and its implication in physiology and human diseases. *Metallomics* **9**, 1376–1388 (2017).

32. Solioz, M. & Stoyanov, J. V. Copper homeostasis in Enterococcus hirae. *FEMS Microbiol Rev* **27**, 183–195 (2003).

33. Cobine, P. *et al.* The Enterococcus hirae copper chaperone CopZ delivers copper(I) to the CopY repressor. *FEBS Lett* **445**, 27–30 (1999).

34. Strausak, D. & Solioz, M. CopY is a copper-inducible repressor of the Enterococcus hirae copper ATPases. *J Biol Chem* **272**, 8932–8936 (1997).

35. Odermatt$, A., Sutert, H., Krapfs, R. & Soliozh, M. Primary Structure of Two P-type ATPases Involved in Copper Homeostasis in Enterococcus hirue*. *THE JOURNAL OF BIOLOGICAL CHEMISTRY* **268**, 12775–12779 (1993).

36. Völlmecke, C., Drees, S. L., Reimann, J., Albers, S. V. & Lübben, M. The ATPases CopA and CopB both contribute to copper resistance of the thermoacidophilic archaeon Sulfolobus solfataricus. *Microbiology (Reading)* **158**, 1622–1633 (2012).

37. Chillappagari, S., Miethke, M., Trip, H., Kuipers, O. P. & Marahiel, M. A. Copper acquisition is mediated by YcnJ and regulated by YcnK and CsoR in Bacillus subtilis. *J Bacteriol* **191**, 2362–2370 (2009).

38. Rubino, J. T. & Franz, K. J. Coordination chemistry of copper proteins: How nature handles a toxic cargo for essential function. *Journal of Inorganic Biochemistry* vol. 107 129–143 Preprint at https://doi.org/10.1016/j.jinorgbio.2011.11.024 (2012).

39. Dell'Acqua, S., Pauleta, S. R., Moura, I. & Moura, J. J. G. The tetranuclear copper active site of nitrous oxide reductase: the CuZ center. *J Biol Inorg Chem* **16**, 183–194 (2011).

40. Horrell, S., Kekilli, D., Strange, R. W. & Hough, M. A. Recent structural insights into the function of copper nitrite reductases. *Metallomics* **9**, 1470–1482 (2017).

41. Castiglione, N., Rinaldo, S., Giardina, G., Stelitano, V. & Cutruzzolà, F. Nitrite and Nitrite Reductases: From Molecular Mechanisms to Significance in Human Health and Disease. *https://home.liebertpub.com/ars* **17**, 684–716 (2012).

42. Rowley, J. *et al.* Chlamydia, gonorrhoea, trichomoniasis and syphilis: global prevalence and incidence estimates, 2016. *Bull World Health Organ* **97**, (2019).

43. Knapp, J. S. & Clark, V. L. Anaerobic growth of Neisseria gonorrhoeae coupled to nitrite reduction. *Infect Immun* **46**, 176–181 (1984).

44. Short, H. B., Clark, V. L., Kellogg, D. S. & Young, F. E. Anaerobic survival of clinical isolates and laboratory strains of Neisseria gonorrhoea: use in transfer and storage. *J Clin Microbiol* **15**, 915–919 (1982).

45. Phillips, N. J. *et al.* Proteomic analysis of Neisseria gonorrhoeae biofilms shows shift to anaerobic respiration and changes in nutrient transport and outermembrane proteins. *PLoS One* **7**, (2012).

46. Costerton, J. W., Stewart, P. S. & Greenberg, E. P. Bacterial biofilms: a common cause of persistent infections. *Science* **284**, 1318–1322 (1999).

47. Mellies, J., Jose, J. & Meyer, T. F. The Neisseria gonorrhoeae gene aniA encodes an inducible nitrite reductase. *Molecular and General Genetics* **256**, 525–532 (1997).

48. Householder, T. C., Fozo, E. M., Cardinale, J. A. & Clark, V. L. Gonococcal Nitric Oxide Reductase Is Encoded by a Single Gene, norB, Which Is Required for Anaerobic Growth and Is Induced by Nitric Oxide. *Infect Immun* **68**, 5241–5246 (2000).

49. Barth, K. R., Isabella, V. M. & Clark, V. L. Biochemical and genomic analysis of the denitrification pathway within the genus Neisseria. *Microbiology (Reading)* **155**, 4093–4103 (2009).

50. Clark, V. L., Knapp, J. S., Thompson, S. & Klimpel, K. W. Presence of antibodies to the major anaerobically induced gonococcal outer membrane protein in sera from patients with gonococcal infections. *Microb Pathog* **5**, 381–390 (1988).

51. Sikora, A. E. *et al.* Peptide Inhibitors Targeting the Neisseria gonorrhoeae Pivotal Anaerobic Respiration Factor AniA. *Antimicrob Agents Chemother* **61**, (2017).

52. Unemo, M. & Shafer, W. M. Antibiotic resistance in Neisseria gonorrhoeae: origin, evolution, and lessons learned for the future. *Ann N Y Acad Sci* **1230**, (2011).

53. Unemo, M. & Nicholas, R. A. Emergence of multidrug-resistant, extensively drug-resistant and untreatable gonorrhea. *Future Microbiol* **7**, 1401–1422 (2012).

54. Boulanger, M. J. & Murphy, M. E. P. Crystal structure of the soluble domain of the major anaerobically induced outer membrane protein (AniA) from pathogenic Neisseria: a new class of copper-containing nitrite reductases. *J Mol Biol* **315**, 1111–1127 (2002).

55. Aas, F. E. *et al.* Cytochrome c-based domain modularity governs genus-level diversification of electron transfer to dissimilatory nitrite reduction. *Environ Microbiol* **17**, 2114–2132 (2015).

56. Cristaldi, J. C. *et al.* Study of the Cys-His bridge electron transfer pathway in a copper-containing nitrite reductase by site-directed mutagenesis, spectroscopic, and computational methods. *Biochim Biophys Acta Gen Subj* **1862**, 752–760 (2018).

57. Li, Y., Hodak, M. & Bernholc, J. Enzymatic mechanism of copper-containing nitrite reductase. *Biochemistry* **54**, 1233–1242 (2015).

58. Li, X., Parker, S., Deeudom, M. & Moir, J. W. Tied down: tethering redox proteins to the outer membrane in Neisseria and other genera. *Biochem Soc Trans* **39**, 1895–1899 (2011).

59. Firth, S. J. The role of the periplasmic Cu metallochaperone AccA in metalating the Cu-dependent nitrite reductase AniA in Neisseria gonorrhoeae. (2023).

60. Schrödinger, L. , & D. W. PyMol. Preprint at http://www.pymol.org/pymol (2020).

61. Jen, F. E. C. *et al.* A genetic screen reveals a periplasmic copper chaperone required for nitrite reductase activity in pathogenic Neisseria. *FASEB J* **29**, 3828–3838 (2015).

62. Llases, M. E., Morgada, M. N. & Vila, A. J. Biochemistry of copper site assembly in heme-copper oxidases: A theme with variations. *International Journal of Molecular Sciences* vol. 20 Preprint at https://doi.org/10.3390/ijms20153830 (2019).

63. Thaqi & Denis. Structural and biochemical characterisation of the periplasmic copper chaperone AccA in Neisseria gonorrhoeae. (2021) doi:10.14264/E960520.

64. Barreiro, D. S., Oliveira, R. N. S. & Pauleta, S. R. Biochemical Characterization of the Copper Nitrite Reductase from Neisseria gonorrhoeae. *Biomolecules* **13**, 1215 (2023).

65. Xu, S., Andrews, D. & Hill, B. C. The affinity of yeast and bacterial SCO proteins for CU(I) and CU(II). A capture and release strategy for copper transfer. *Biochem Biophys Rep* **4**, 10–19 (2015).

66. Chelators. https://www.sigmaaldrich.com/GB/en/technical-documents/technical-article/protein-biology/protein-purification/chelators.

67. Young, T. R. *et al.* A set of robust fluorescent peptide probes for quantification of Cu(ii) binding affinities in the micromolar to femtomolar range. *Metallomics* **7**, 567–578 (2015).

68. Liu, T., Reyes-Caballero, H., Li, C., Scott, R. A. & Giedroc, D. P. Multiple metal binding domains enhance the Zn(II) selectivity of the divalent metal ion transporter AztA. *Biochemistry* **46**, 11057–11068 (2007).

69. Ghosh, S. *et al.* Thermodynamic equilibrium between blue and green copper sites and the role of the protein in controlling function. *Proc Natl Acad Sci U S A* **106**, 4969–4974 (2009).

70. Solomon, E. I., Szilagyi, R. K., DeBeer George, S. & Basumallick, L. Electronic Structures of Metal Sites in Proteins and Models: Contributions to Function in Blue Copper Proteins. *Chem Rev* **104**, 419–458 (2004).

71. Adman, E. T., Godden, J. W. & Turley, S. The structure of copper-nitrite reductase from Achromobacter cycloclastes at five pH values, with NO2- bound and with type II copper depleted. *Journal of Biological Chemistry* **270**, 27458–27474 (1995).

72. Mazmanian, K., Sargsyan, K., Grauffel, C., Dudev, T. & Lim, C. Preferred Hydrogen-Bonding Partners of Cysteine: Implications for Regulating Cys Functions. *Journal of Physical Chemistry B* **120**, 10288–10296 (2016).

73. Rao Mundlapati, V., Ghosh, S., Bhattacherjee, A., Tiwari, P. & Biswal, H. S. Critical assessment of the strength of hydrogen bonds between the sulfur atom of methionine/cysteine and backbone amides in proteins. *Journal of Physical Chemistry Letters* **6**, 1385–1389 (2015).

74. Berman, H. M. *et al.* The Protein Data Bank. *Nucleic Acids Res* **28**, 235–242 (2000).

75. Hoehn, G. T. & Clark, V. L. Isolation and Nucleotide Sequence of the Gene (aniA) Encoding the Major Anaerobically Induced Outer Membrane Protein of Neisseria gonorrhoeae. *INFECrION AND IMMUNITY* 4695–4703 (1992).

76. Kuznetsova, I. M., Turoverov, K. K. & Uversky, V. N. What macromolecular crowding can do to a protein. *Int J Mol Sci* **15**, 23090–23140 (2014).

77. Petasis, D. T. & Hendrich, M. P. Quantitative Interpretation of Multifrequency Multimode EPR Spectra of Metal Containing Proteins, Enzymes, and Biomimetic Complexes. *Methods Enzymol* **563**, 171–208 (2015).

78. Tabak, M., Sartor, G., Neyroz, P., Spisni, A. & Cavatorta, P. Interaction of copper and nickel ions with tryptophan and glyciltryptophan: Time resolved flourescence study. *J Lumin* **46**, 291–299 (1990).

79. Ungor, D., Bélteki, R., Horváth, K., Dömötör, O. & Csapó, E. Fluorescence Quenching of Tyrosine-Ag Nanoclusters by Metal Ions: Analytical and Physicochemical Assessment. *Int J Mol Sci* **23**, (2022).

80. Möller, M. & Denicola, A. Protein tryptophan accessibility studied by fluorescence quenching. *Biochemistry and Molecular Biology Education* **30**, 175–178 (2002).

81. Zhdanova, N. G. *et al.* Tyrosine fluorescence probing of the surfactant-induced conformational changes of albumin. *Photochem Photobiol Sci* **14**, 897–908 (2015).

82. Sethuraman, S. & Rajendran, K. Multicharacteristic Behavior of Tyrosine Present in the Microdomains of the Macromolecule Gum Arabic at Various pH Conditions. *ACS Omega* **3**, 17602–17609 (2018).

83. Mozo-Villarías, A. Second derivative fluorescence spectroscopy of tryptophan in proteins. *J Biochem Biophys Methods* **50**, 163–178 (2002).

84. Asor, R. & Kukura, P. Characterising biomolecular interactions and dynamics with mass photometry. *Curr Opin Chem Biol* **68**, 102132 (2022).

85. Soltermann, F. *et al.* Quantifying Protein–Protein Interactions by Molecular Counting with Mass Photometry. *Angew Chem Int Ed Engl* **59**, 10774 (2020).

86. Foley, E. D. B., Kushwah, M. S., Young, G. & Kukura, P. Mass photometry enables label-free tracking and mass measurement of single proteins on lipid bilayers. *Nature Methods 2021 18:10* **18**, 1247–1252 (2021).

87. Bertini, I. & Pierattelli, R. Copper(II) proteins are amenable for NMR investigations. *Pure and Applied Chemistry* **76**, 321–333 (2004).

88. Dreydoppel, M., Balbach, J. & Weininger, U. Monitoring protein unfolding transitions by NMR-spectroscopy. *J Biomol NMR* **76**, 3–15 (2022).

89. Lipchock, J. M. & Loria, J. P. Monitoring molecular interactions by NMR. *Methods Mol Biol* **490**, 115–134 (2009).

90. Jarymowycz, V. A. & Stone, M. J. Fast time scale dynamics of protein backbones: NMR relaxation methods, applications, and functional consequences. *Chem Rev* **106**, 1624–1671 (2006).

91. Hu, Y. *et al.* NMR-Based Methods for Protein Analysis. *Anal Chem* **93**, 1866–1879 (2021).

92. Liang, B. & Tamm, L. K. Structure of outer membrane protein G by solution NMR spectroscopy. *Proc Natl Acad Sci U S A* **104**, 16140 (2007).

93. Horrell, S., Kekilli, D., Strange, R. W. & Hough, M. A. Recent structural insights into the function of copper nitrite reductases. *Metallomics* **9**, 1470–1482 (2017).

94. Wu, H. J. *et al.* Azurin of pathogenic Neisseria spp. is involved in defense against hydrogen peroxide and survival within cervical epithelial cells. *Infect Immun* **73**, 8444–8448 (2005).

95. Gotschlich, E. C. & Seiff, M. E. Identification and gene structure of an azurin-like protein with a lipoprotein signal peptide in Neisseria gonorrhoeae. *FEMS Microbiol Lett* **43**, 253–255 (1987).

96. Branch, A. H., Stoudenmire, J. L., Seib, K. L. & Cornelissen, C. N. Acclimation to Nutritional Immunity and Metal Intoxication Requires Zinc, Manganese, and Copper Homeostasis in the Pathogenic Neisseriae. *Front Cell Infect Microbiol* **12**, 909888 (2022).

97. Miethke, M. & Skerra, A. Neutrophil Gelatinase-Associated Lipocalin Expresses Antimicrobial Activity by Interfering with l-Norepinephrine-Mediated Bacterial Iron Acquisition. *Antimicrob Agents Chemother* **54**, 1580 (2010).